

**REVIEW OF AERONAUTICAL FATIGUE
INVESTIGATIONS IN JAPAN
DURING THE PERIOD JUNE 2015 TO MAY 2017**

Edited by

Nobuo Takeda
The University of Tokyo

Shigeru Machida
Takao Okada
Japan Aerospace Exploration Agency

For Presentation at the 35rd Conference of
the International Committee on Aeronautical Fatigue and Structural Integrity

Nagoya Japan, 5-6 June, 2017

CONTENTS

	page
1. INTRODUCTION	1
 2. FATIGUE AND FAILURE IN METALLIC MATERIALS AND COMPONENTS	
2.1 Fatigue Crack Propagation Resistance Relevant to Microstructure in A Friction Stirred Welded Ti-6Al-4V Titanium Alloy Joint	3
2.2 Fatigue crack growth behavior in residual stress field formed by friction stir welding	3
2.3 Fatigue life assessment of welded joints under step loading using equivalent crack length method	4
2.4 Multiaxial fatigue life assessment using cruciform specimen for Ti-6Al-4V	5
 3. FATIGUE AND FAILURE IN COMPOSITE MATERIALS AND COMPONENTS	
3.1 Life prediction by simulation of transverse crack initiation in CFRTP laminates under fatigue loading	7
3.2 Fatigue life prediction of thick CFRP laminates with toughened interlaminar layers in the out-of-plane direction at different stress ratios	7
3.3 Fatigue Modeling for Intralaminar Damage Evolution in Composite Laminates Based on Damage State Variables	8
3.4 Arresting Fatigue Crack in Composite Bonded Joint using Fiber-Reinforcement Design Feature	8
3.5 High-functioning Composite T-joint using Atypical Stacking Sequence and Deltoid Structure	9
3.6 Effect of taper angles on delamination strength of tapered composite laminates	10
3.7 Tokyo Metropolitan University - JAXA Collaborative Research on Composite Wing Structures	11
3.8 Fatigue Test Trial of CFRP Coupon Specimens	12
 4. STRUCTURAL HEALTH MONITORING	
4.1 Ultra-lightweight composite structures designed based on SHM and rapid repair system	13
4.2 Optical Fiber Sensor based Impact Detection System for Aircraft Structures	13
4.3 Development of ultrasonic wave based structural health monitoring system for practical use	14
 5. LIFE EVALUATION ANALYSIS	
5.1 Application of Bayesian Method for Determining a Simple Reliability Index for Composite Material Strength	16
 6. FULL SCALE TESTING	
6.1 Structural Damage and Repair Assessment for MRJ Aircraft	18
6.2 Full Scale Strength Tests of XP-1 Aircraft	19
6.3 Full Scale Strength Tests of XC-2 Aircraft	19

6.4 Full Scale Static Test of X-2 Advanced Technology Demonstrator	20
7. MISCELLANEOUS	
7.1 An amphibian and the concept of its derivative model for firefighting application	21
7.2 Visualization of strain distribution and portent of destruction in structural material through mechanoluminescence	21
7.3 Development of Analysis and Test Methods for Lightning Strike on CFRP structures	22
7.4 Introduction of Effort About Construction for Fractography Database in Japan	22
7.5 Aircraft Accident Investigation	25
ACKNOWLEDGEMENTS	25
TABLES AND FIGURES	26

1. INTRODUCTION

Nobuo Takeda, National Delegate, The University of Tokyo

This review summarizes the papers on the study of aeronautical fatigue, structural integrity and related themes conducted in Japan during June 2015 to May 2017.

The papers were contributed by following organizations:

Japan Aerospace Exploration Agency (JAXA)
Acquisition, Technology & Logistics Agency (ATLA)
R&D Institute of Metals and Composites for Future Industries (RIMCOF)
National Institute of Occupational Safety and Health, Japan (JNIOSH)
Mitsubishi Heavy Industries, Ltd. (MHI)
Mitsubishi Aircraft Corporation
Kawasaki Heavy Industries, Ltd. (KHI)
SUBARU CORPORATION
IHI Corporations
IHI Aerospace Co., Ltd.
ShinMaywa Industries, Ltd.
The University of Tokyo
Doshisha University
Kyushu Institute of Technology
Tokyo Metropolitan University
Waseda University

The general activities on aircraft development program in Japan during 2015 to 2017 is summarized as follows:

- The development of MRJ (Mitsubishi Regional Jet, 70-to 90-seat regional jets) aircraft is in the final stage and various steps for the certification is being made. The first flight was successfully completed in November, 2015. The production is underway at Mitsubishi Aircraft Corporation in Nagoya. As of September 2016 more than 400 of these jets (including options and purchase rights) have been ordered.
- Japanese companies are playing an important role in the global joint development of the Trent1000, GENx and other engines for Boeing787 and are taking part as the manufacturer of the low pressure turbine components of GE9X engines for Boeing777X. And also, they are also participating in global joint development of the PW1100G-JM engine for the Airbus A320neo to achieve fuel-efficiency, low-pollution, and noise-reduction, with P&W taking the lead.
- Simultaneous development activities began in 2001 for XP-1 Maritime Patrol Aircraft and XC-2 Transport Aircraft to be used as successor models for the P-3C and the C-1, respectively. Multi-utilization was the key issue in order to reduce overall development costs. XP-1 Maritime Patrol Aircraft succeeded in the first flight in September 2007 and started delivering to the base from March 2013. XC-2 Transport Aircraft successfully completed its first flight in January 2010 and delivery to the base will start soon.
- R&D Institute of Metals and Composites for Future Industries (RIMCOF) was established in July 2016 to promote R&D efficiency in materials and structures development for new aircraft in collaboration with industries, universities and national laboratories. RIMCOF is responsible to operate “Civil Aviation Fundamental Technology Program -Advanced Materials & Process Development for Next-Generation Aircraft Structures” supported by NEDO (New Energy and Industrial Technology Development Agency). The program includes three projects on (1) Practical Use of Structure Health Monitoring (SHM) for Composite Aircraft, (2) High Rate Manufacturing of CFRP Parts, and (3) Material Development and Processing of Next-Generation Magnesium Alloys.
- “Structural Materials for Innovation” (SM⁴I) Project started in 2014 as a part of SIP (Cross-ministerial Strategic Innovation Promotion Program) supported by the Council for Science, Technology and Innovation (CSTI) of the Cabinet Office, Japan. New material development is underway in the following areas; (1) High Rate Production CFRP Materials, (2) High Temperature Alloys and Intermetallic Compounds, (3) Ceramic Coatings and Ceramic Matrix Composites (CMC), and (4) Materials Integration. The CFRP materials in development covers, OoA (Out-of-autoclave) prepregs, Advanced Resin Transfer Molding (RTM) materials, Advanced Thermoplastic prepregs, High

Temperature Polyimide CFRP prepregs. Process and life cycle monitoring technologies are utilized to establish the manufacturing modeling codes for cost effective material certification.

2 FATIGUE AND FAILURE IN METALLIC MATERIALS AND COMPONENTS

2.1 Fatigue Crack Propagation Resistance Relevant to Microstructure in A Friction Stir Welded Ti-6Al-4V Titanium Alloy Joint.

M. Okazaki¹, M. Muzvidziwa², S. Hirano³

¹Nagaoka University of Technology 1603-1 Kamitomioka-machi, Nagaoka-shi, Niigata 940-2188, Japan

²Hitachi Automotive Systems Co., Japan

³Hitachi Research Lab., Hitachi 319-1292, Japan

Development of tools applicable to friction stir welding (FSW) and friction stir processing (FSP) of materials with high softening temperatures has recently promoted research in processing of titanium alloys via these techniques. The FSW technology is relatively new and offers a number of advantages over conventional welding techniques namely higher process speeds, elimination of filler materials and minimal shrinkage and post weld distortion. As such, a considerable amount of work has been done to optimise and understand the damage behavior of friction stir welded (FSWed) alloys. On considering the reliability of the FSWed components, one of critical issue is to understand the roles of microstructure gradation, hardness distribution and residual stresses.

In this work, the role of the microstructure and residual stresses on the FCP of a FSWed 6-4 titanium alloy were investigated. Initially, the microstructural development in the weld was studied and correlated to the measured monotonic properties of the weld. FCP tests on CT specimens containing initial notches in the stirred zone (SZ) and parallel to weld direction were carried out with subsequent analysis based on the microstructure and residual stresses obtained through the X-ray diffraction (XRD) method. The residual stresses were measured in the base metal (BM), SZ, advancing side (AS) and also on the retreating side (RS) of the weld.

The starting material in this work was a FSWed plate of a Ti-6Al-4V alloy jointed through a single pass in a butt joint configuration (Fig. 1(a)). The fatigue crack growth rates in the base metal and welded area were measured on compact tension (CT) specimens with initial notches in the base metal and the stirred zone respectively, by extracting the miniature CT specimens shown in Fig. 1(b). They were precisely extracted from a depth of 0.4mm from the top surface by EDM from both the welded area. The fatigue crack propagation (FCP) tests were carried out under ambient conditions, a load ratio, R , of 0.6 and loading frequency of 20Hz. The crack length was monitored and measured through a travelling digital microscope continuously focused on the specimen surface. The residual stresses in the base metal and the welded area were measure through the $\text{Sin}^2\psi$ method of the X-ray diffraction (XRD) technique.

The experimental results indicated that the local resistance to fatigue crack propagation was different depending on the site where the crack propagated (Fig. 2). Significant kinking of the cracks towards the retreating side was also observed in FSW specimens but not in the BM. The effect of the kinking on the effective crack driving force, ΔK_{eff} , at the crack tip was factored in using the coplanar maximum strain energy release rate theory, after which a small reduction in the differences between the FCP rates of the BM and the FSW was obtained. The difference in the FCP rate between the BM and the FSW after application of the ΔK_{eff} was discussed with regards to the microstructural evolution; refinement of the microstructure gives small sized α colonies and slip lengths which could result in the lower FCP rates. Residual stresses obtained through XRD could also be used to understand the FCP behavior in the FSW specimens. The in-plane residual stresses were found to be predominantly tensile but with significant variations across the weld. Considering the tensile residual stresses in the SZ and the lower FCP rates, it was postulated that for the current material, the influence of microstructure on the FCP was predominant over that of the residual stress. It was also shown through considerations of the heterogeneity in maximum shear stress components that these variations could play a role in the crack kinking and thus the FCP behavior in the FSW.

2.2 Fatigue crack growth behavior in residual stress field formed by friction stir welding

Takao Okada¹, Shigeru Machida¹, Toshiya Nakamura¹, Motoo Asakawa²

¹Japan Aerospace Exploration Agency, Japan

²Former Waseda University, Japan

It is well known that the residual stress affects the structural behavior such as fatigue life and fatigue crack growth behavior. And fatigue crack growth behavior in the residual stress field is one of the imperative properties to be understood in order to accurately design the structure.

Friction stir welding is one of the welding procedure which is expected to be applied to the aircraft structure. Friction stir welding stirs and heats the materials to be joined and residual stress distribution is introduced along the weld line. Many of the properties for friction stir welding has to be well known and extensive researches have been conducted. And the research for evaluation of fatigue crack growth behavior in FSW(Friction stir welded) joint also have been conducted¹⁻⁴⁾.

The crack propagation tests were conducted to evaluate the effect of stress range on crack growth rate in FSW 2024-T3 aluminum alloy. The crack growth rate of the base material is compared in order to evaluate the change of the crack growth around the weld line. The crack growth rate of the FSW joint is also compared with the $da/dN-\Delta K_{eff}$ curve.

The test results confirm that the crack growth rate is accelerate around the tensile residual stress region and the crack growth rate for both side are mostly close to the $da/dN-\Delta K_{eff}$ curve for $\Delta\sigma = 25$ Mpa (Fig. 3). The peak of the acceleration is not at the location of maximum tensile residual stress but some distance away from the center of the specimen. The relationship between the modified stress ratio and crack growth acceleration in FSW panels is evaluated by an analysis using the stress intensity factor range with and without residual stress and the result is shown in Fig. 4. The modified stress ratio identifies that the ratio is greater as lower the stress amplitude. It becomes about 0.8 for $\Delta\sigma = 25$ MPa and is considered that the crack is fully opened. Same as the location of the maximum acceleration, the location of the maximum modified stress ratio shifts some distance away from the center of the specimen.

References

- 1) H.J.K. Lemmen, R.C. Alderliesten, R. Benedictus, "Macro and microscopic observation of fatigue crack growth in friction stir welded aluminum joints", *Engineering Fracture Mechanics*, Vol. 78, 2011, pp. 930-943.
- 2) Y. Ma, and P. Irving, "Residual Stress Effects and Fatigue Behavior of Friction-Stir-Welded 2198-T8 Al-Li Alloy Joints", *Journal of Aircraft*, Vol. 48, No. 4, 2011, pp. 1238-1244.
- 3) T. Okada, S. Machida T. Nakamura, H. Tanaka, K. Kuwayama and M. Asakawa, "Fatigue crack growth of friction stir welded Aluminum alloy", *Journal of Aircraft*, Accepted for publication.
- 4) L. Frantini, S. Pasta, A. Reynolds, "Fatigue crack growth in 2024-T351 friction stir welded joints: Longitudinal residual stress and microstructural effects", *Int. Journal of fatigue*, Vol. 31, 2009, pp.495-500.

2.3 Fatigue life assessment of welded joints under step loading using equivalent crack length method

Takao Murakami¹ and Yoichi Yamashita¹

¹ IHI Corporation

Since a fatigue failure of welded structures may cause serious accidents, a number of researches have been conducted on fatigue life assessment methodology to avoid accidents due to fatigue failure. S-N curve is usually required to estimate fatigue life. However, we have to conduct fatigue test using many specimens to obtain S-N curve. Equivalent crack length method¹⁾, which enables us to obtain S-N curve from only one experimental data of fatigue test, is introduced in this paper. Equivalent crack length method assumes a crack of which length is a_0 in the infinite flat plate, instead of assuming the realistic crack length contained in the corresponding welded joints (Fig. 5). When a_0 is given, the crack propagation life under constant amplitude loading conditions can be calculated by integration of Paris' law, and the S-N curve can be determined.

Estimation of S-N curve by using equivalent crack length method was conducted, and the assessments results were compared with the experimental results. Under constant amplitude loading conditions, estimated S-N curves derived from one experimental data point were consistent with the experimental results, same as reported in the literature¹⁾. Under step loading conditions, for some cases, fatigue lives estimated by using equivalent crack method was longer than that of experimental results. Stress concentration of the surface

largely affects the fatigue crack growth rate when the crack size is small. However, stress concentration effects are not considered in the calculation of stress intensity factor range. Therefore, stress intensity factor range, ΔK , was underestimated in the short crack length range, and as a result, calculated fatigue lives were overestimated. When ΔK_{th} is ignored, nearly all estimated fatigue lives fall within the factor of two in life (Fig. 6).

Further, the relationship between a_0 and the stress concentration factor, K_t , was investigated, in order to predict fatigue life only by K_t estimation. For example, K_t can be calculated from FEA (finite element method), and in this case, fatigue life is able to predict without using experimental results. M.M. Pedersen et al⁽²⁾ calculated K_t by using finite element method, for various kinds of specimens which have welded joints. a_0 was calculated for each kinds of specimens, and the relationship was expressed as one equation of $a_0[mm] = 0.015 \cdot (K_t - 1)^m + 0.045$. Sasaki⁽³⁾ had studied for the effect of grinding treatment at the weld toe for longitudinal gusset welded specimens. K_t , which differs depending on the geometry of weld toe, is calculated by FEA. S-N curve was estimated from K_t , and the estimation results well accorded with the experimental results (Fig. 7).

References

- 1) Eeva Mikkola, Yukitaka Murakami and Gary Marquis. (2014) "Fatigue life assessment of welded joints by the equivalent crack length method", *Procedia Materials Science* 3, 1822-1827
- 2) M.M. Pedersen, O.O. Mouritsen, M.R. Hansen, J.G. Andersen, J. Wenderby. (2010) "Re-analysis of fatigue data for welded joints using the notch stress approach", *Int J Fatigue* 32, 1620-1626
- 3) Y. Sasaki. (2013) "INFLUENCE OF GRINDING DEPTH AND AREA ON FATIGUE STRENGTH OF OUT-OF-PLANE GUSSET JOINTS WITH FINISHED WELD TOES" Hosei University Repository Vol.2 (in Japanese)

2.4 Multiaxial fatigue life assessment using cruciform specimen for Ti-6Al-4V

Hiroshi Nakamura^{1*}, David Backman², Min Liao², Takuya Yoden¹, Tomoyuki Tanaka¹

¹ IHI Corporation, Aero-Engine & Space Operations, Japan

² National Research Council Canada, Canada

Ti-6Al-4V is often used to manufacture rotating components on aero engines; specifically those from the low temperature sections such as fan and compressor disks and blade parts. This is because of the excellent specific static strength and fatigue properties of Ti-6Al-4V. Rotating components are routinely subjected to complicated cyclic stresses due to variable loading and structural discontinuity of the components. This situation results in multiaxial low cycle fatigue (LCF) damage during operation. Multiaxial fatigue life modeling is an essential tool in rotating component design because structural integrity of the turbine components is dominated by fatigue failure. Static yield theory is often used in a multiaxial fatigue life model. It has been reasoned that since fatigue damage is controlled by plastic deformation, the yield criteria should be adequate to describe fatigue behavior. The most common yield criteria are the equivalent stress based on von Mises theory and the maximum principal stress. Each life model has some limitations on its applicability, depending on the component geometry and material constituents. This paper conducts an assessment of multiaxial fatigue life models for some Ti-6Al-4V specimens subject to biaxial testing, and an appropriate model is determined and suggested to predict LCF lives.

To investigate fatigue life under multiaxial stress states, load controlled biaxial tests have been conducted using a cruciform specimen. Geometries of the cruciform specimens are shown in Figure 8. Two types of cruciform specimens were designed in this study. One is a cruciform with a central notch, and the other is a cruciform with a smooth central gauge region. Figure 9 shows the finite element analysis stress results of the specimens. Local peak stress occur inside the central notch while a uniform stress state could be seen on the gauge region of the smooth cruciform. The fatigue tests have been carried out by National Research Council Canada (NRC) using a planar biaxial MTS test frame shown in Figure 10. This test program is still undergoing in partnership between NRC and IHI Corporation.

Biaxial load ratio (BR) for the notch cruciform was 0.9 and BR for the smooth cruciforms were -0.9, -0.1, 0.7

and 0.9. The LCF tests have been conducted at room temperature and ambient air. Strain and crack growth were monitored using digital image correlation and thermoelastic stress analysis techniques. Life predictions for the notch cruciform using Mises stress and principal stress show similar results. This is because the biaxial stress ratio at the peak stress location of the notch cruciform is close to 0, i.e., uniaxial stress state. Figure 11 shows S-N diagrams using the von Mises stress and the maximum principal stress. The Mises stress is conservative to assess LCF life under negative biaxial ratio and life prediction using Mises stress shows a large scatter. The maximum principal stress is slightly conservative to assess LCF life under positive biaxial ratio. Overall, using the maximum principal stress is a more accurate method to determine fatigue life and it covers a wide range of biaxial ratios in LCF life prediction for Ti-6Al-4V.

3. FATIGUE AND FAILURE IN COMPOSITE MATERIALS AND COMPONENTS

3.1 Life prediction by simulation of transverse crack initiation in CFRTP laminates under fatigue loading

Atsushi Hosoi¹, Taichi Watanabe¹, Akiya Ozeki¹, Motoki Terauchi¹,

Akira Kobiki², Hiroyuki Kawada^{1,3}

¹Waseda University, Japan

²IHI Corporation, Japan

³Kagami Memorial Research Institute for Material Science and Technology, Waseda University, Japan

The impact resistance of carbon fiber reinforced thermoplastic (CFRTP) composites is greater than that of carbon fiber reinforced thermoset (CFRTS) composites, so that applications using CFRTP composites to aircraft components will continue to be further developed. On the other hand, the fatigue strength of the CFRTP composites decreases more than that of the CFRTS composites because of the ductile properties of matrix resin in the CFRTP composites. It is important to evaluate the fatigue life of CFRTP composites comprehensively for more precise fatigue design although the damage tolerant design is mainly adapted for the aircraft design. Especially, to evaluate damage initiation gives the important design guidelines from the viewpoint of the safe life design. Therefore, the fatigue life to the transverse crack initiation was evaluated using CFRTP cross-ply $[0/90_4]_s$ laminates and 90° unidirectional laminates in this study. Fatigue tests were conducted under the test conditions of the stress ratio of $R = 0.1$ and the frequency of $f = 5$ Hz and the damage growth behavior was observed with optical microscopy and soft X-ray photography. The initiation of transverse crack in the cross-ply $[0/90_4]_s$ laminates and the fatigue lives of 90° unidirectional laminates and thermoplastic matrix materials are evaluated experimentally. To evaluate the fatigue life to crack initiation analytically, numerical simulation was carried out based on the fatigue life prediction model considered the mean stress effect, Smith-Watson-Topper (SWT) model. The principal stresses applied in the matrix resin of the composites per 1 cycle were calculated by the finite element analysis. The fatigue life to fracture of matrix resin in the CFRTP composites was calculated as damage initiation of the composites assuming that the fracture of matrix resin follows the SWT model. Figure 12 shows the numerical simulation result of the fatigue life distribution in the element model of the 90° unidirectional laminates applied maximum strain of $\varepsilon_{\max} = 0.5\%$. Red area shows the fatigue life is short and that is damage initiation cycles and area. It is found that the damage initiates at the vicinity of the interface between fiber and matrix resin and at the narrow space between fibers from the results. Figure 13 showed the experimental and analytical results of S-N curve of 90° unidirectional laminates. Although the analytical results estimated the fatigue life slightly longer than the experimental results, the analytical results showed good agreement with the experimental results in the tendency of the fatigue life.

3.2 Fatigue life prediction of thick CFRP laminates with toughened interlaminar layers in the out-of-plane direction at different stress ratios

Atsushi Hosoi¹, Shiwon Tsuge², Sen Seki², Yuzo Fujita³ and Hiroyuki Kawada^{1,4}

¹ Department of Applied Mechanics and Aerospace Engineering, Waseda University

² Graduate School of Fundamental Science and Engineering, Waseda University

³ Composite Materials Research Laboratories, Toray Industries, Inc.

⁴ Kagami Memorial Research Institute for Material Science and Technology, Waseda University, Japan

The fatigue life of thick carbon fiber reinforced plastic (CFRP) laminates with toughened interlaminar layers in the out-of-plane direction was predicted at different stress ratios. CFRPs begin to be applied for the large structural members in not only airplane but also automobiles, wind turbine blades, tidal turbine blades and so on. The mechanical properties of CFRP laminates in the out-of-plane direction, however, are inferior to those in the in-plane directions because fibers in the laminates are generally not oriented in the out-of-plane direction. Thus, it is essential to evaluate the mechanical properties of thick CFRP laminates in the out-of-plane direction for establishing their long-term durability and reliability. In addition, a method to predict the fatigue life of thick CFRP laminates in the out-of-plane direction has not been established. Therefore, a model was proposed to predict the fatigue life of the thick CFRP laminates in the out-of-plane direction considered the effect of stress ratio, and the fatigue properties of the thick CFRP laminates were evaluated with the

constant-life diagram derived from the proposed model. In this study, the unidirectional thick CFRP laminates, which pile up 88 layers of the prepreg with toughened layer, T800S/3900-2B, were formed with an autoclave. The fiber volume fraction of the laminates is $V_f = 56\%$, and the cure temperature is 453 K. The specimens were machined from the approximately 17 mm thick laminates. The shape of specimens is a cylinder solid with a narrow part like a spool shape. The diameters of the minimum and maximum cross-section surfaces are 18.75 mm and 25.0 mm, respectively as shown in Fig. 14. Metal tabs were bonded to the upper and lower surfaces of the specimen. Fatigue tests were run at a frequency of $f = 5$ Hz and stress ratio of $R = 0.1, -1, -3$ or -6 . The fracture surface of the specimens was observed with optical microscopy and scanning electron microscopy. Figure 15 shows the S-N curve, which indicates the relationship between the maximum stress on the surface of the fiber layer at the minimum cross-section and the number of cycles to failure. The fatigue life became shorter as the stress ratio became smaller, i.e. as the absolute values of the compressive stress became higher. The lines show the results calculated with the prediction model. The analytical results showed good agreement with experimental results. Then, the constant-life curve derived from the proposed model. The results make it possible to perform quantitative safety design for fatigue in the out-of-plane direction of thick CFRP laminates with toughened interlaminar layers.

3.3 Fatigue Modeling for Intralaminar Damage Evolution in Composite Laminates Based on Damage State Variables

Tomohiro, Yokozeki
The University of Tokyo, Japan
 E-mail address: yokozeki@aastr.t.u-tokyo.ac.jp

The aim of this study is to deal with the simulation of intralaminar fatigue damage in unidirectional composites under complex loadings. The proposed damage model for fatigue is based on stiffness degradation laws accounting for the stress and damage levels combined with the ‘damage’ cycle jump approach. The initial static damage of the material is simulated by using the Ladevèze damage model and the evolution law for damage state variables accounting for stiffness degradation due to intralaminar damages is modeled by thermodynamic forces defined in Ladevèze model. This approach is implemented into FEM software. The simulation based on this intralaminar fatigue damage model is compared with test data to identify the fatigue parameters of the stiffness degradation law. Finally, the validation is conducted using the flexural fatigue test results as shown in Fig. 16, indicating that this overall procedure for fatigue life prediction is demonstrated to be cost efficient at industrial level.

3.4 Arresting Fatigue Crack in Composite Bonded Joint using Fiber-Reinforcement Design Feature

Shu Minakuchi and Nobuo Takeda
 The University of Tokyo, Japan

Even though bonded joints potentially possess clear advantages over traditional bolted joints, composite primary structures in aircraft are currently assembled with several hundreds of thousands of bolts. This is because existing bonding technologies and related non-destructive inspection techniques are unreliable and cannot satisfy airworthiness requirements. It is recognized that development of new design features that stop cracks from growing above a critical size is one of the key steps to realization of boltless composite structures [1]. We have been proposing a new crack arrester concept based on fiber-reinforcement [2]. The basic idea is that continuous high-strength fibers are introduced in the adhesive layer and their massive bridging suppresses crack propagation. One example is depicted in Fig. 17. This x-type crack arrester consists of 0° and 90° composite layers cured during the bonding process. The 90° layer is inserted between the 0° layers that are interlocked during the layup process. When a crack including the one propagating in the adherend approaches the arrester, the crack is robustly entrapped in the arrester by employing the surface feature of the adherends. When the crack passes through the crossing part, one 0° layer bridges the crack and suppresses the crack opening (Fig. 17 A). Furthermore, the 90° layer, which is constrained by the other side 0° layer, prevents the bridging layer from peeling off (Fig. 17 B). So when the crack further propagates, fibers break in the 0° or 90° layers and significant energy is absorbed.

Following our previous study evaluating the arrester performance under mode I and mode II static loading conditions [2, 3], this current study conducted crack lap shear (CLS) fatigue tests to evaluate the performance under a realistic condition. CLS testing simulates a loading condition near stiffener run-out and mixed-mode crack propagation is induced [1]. Figure 18 (a) shows the CLS test setup. The specimen total length was 320mm and the width was 25mm. Two CLS test specimens with different arrester configurations were tested to clarify the effect of arrester thickness on crack stopping performance. The fatigue tests were conducted using a servo-hydraulic test machine at 8 Hz sinusoidal with a load ratio R of 0.1 (tension-tension loading). The maximum load was 15kN that corresponded to the strap strain of $5400\mu\epsilon$. Additionally specimens without the arrester were fabricated by simply introducing 0° layers in the adhesive layer and tested for comparison. Figure 18 (b) shows the fatigue crack growth curves obtained in the CLS tests. In the specimens without the arrester, cracks propagated with constant growth rates until the length reached 100mm. Meanwhile, the specimens with the arrester exhibited almost the same crack propagation behavior at the beginning of the tests as the specimens without the arrester, however the crack growth rate decreased when the crack tip passed through the crossing part of the arrester (i.e., crack length of 30mm). In the specimen with thinner arrester (0-1_90-1), the crack growth rate gradually decreased after the crack tip passed through the crossing part of the arrester and the crack propagated at a quite slow constant rate after the crack length exceeded 40mm. In contrast, in the specimen with thicker arrester (0-3_90-2), the crack growth rate dramatically decreased as the crack tip reached the crossing part of the arrester and the crack stopped before its length reached 40mm. This result suggests that as the arrester thickness increases the crack growth rate decreases and the crack length at which the arresting effect becomes significant changes.

Finally finite element analysis was conducted to understand the crack arresting mechanism. Figure 19 shows the deformation around the crack tip calculated. In the model with the arrester, the 90° layer constrained by the two 0° layers bridged the crack, suppressing opening of the crack and the secondary bending deformation due to the eccentric load path between the strap and the overlap part. As a result, both mode-I and mode-II energy release rates significantly reduced and the crack growth rate in the CLS fatigue test decreased after the crack tip passed through the crossing part of the arrester.

References

- [1] T. Kruse, T. Körwien, S. Heckner and M. Geistbeck. (2015). Bonding of CFRP primary aerospace structures – crackstopping in composite bonded joints under fatigue. *Proceedings of The 20th International Conference on Composite Materials*, 2219-1.
- [2] S. Minakuchi. (2015). Fiber-reinforcement-based crack arrester for composite bonded joints. *Proceedings of The 20th International Conference on Composite Materials*, 2118-4.
- [3] S. Minakuchi and N. Takeda. (2016). Arresting crack in composite bonded joint using fiber-reinforcement-based design feature. *Proceedings of 17th European Conference on Composite Materials*, WED-1_STO_3.20-03.

3.5 High-functioning Composite T-joint using Atypical Stacking Sequence and Deltoid Structure

Shinsaku Hisada¹, Kazunori Takagaki¹, Shu Minakuchi¹, and Nobuo Takeda¹

¹The University of Tokyo, Japan

One of the difficulties in composite structural application is joining components. T-joint is one of the important elements in aircraft structures that transfers load between vertical and horizontal panels. T-joint is composed of two L-shaped parts, skin laminate, and deltoid region. T-joint often fails at low load in deltoid and corner regions because of its low through-thickness properties and process-induced defects. In previous work, Burns et al. proposed novel ply design approaches to increase the strength of T-joint. Trask et al. investigated the influence of process-induced defects in deltoid region on the failure of composite T-joint. In this current study, we proposed T-joint designs using atypical stacking sequence to simultaneously enhance strength and shape-stability. Asymmetric laminate composites usually exhibit large distortion in the out-of-plane direction after cure due to orthotropic material properties. However, in T-joints, the stacking sequence of whole stiffener becomes symmetric even if each L-shaped part is an asymmetric laminate (Figure 20). In addition, deformation in flange is restrained by the skin laminate. Therefore, spring-in deformation in T-joints can be reduced without distortion in the flanges. We evaluated the effectiveness of the design using a

three-dimensional shape measurement system. It was revealed that spring-in deformation was reduced without distortion in flanges using asymmetric lamination. Moreover, we proposed new deltoid structures to improve the strength of T-joint. Figure 21 represents the numerical result of the strain in the lateral direction under tensile load as seen in the global coordinate system. When the stiffener laminate is pulled up, fracture region deforms in the lateral direction due to the constraint of the 0° layers at the surface side and skin bending. This deformation causes out-of-plane stresses, especially out-of-plane shear stress, leading to T-joint's fracture. Therefore, restraint of lateral deformation in the fracture region is needed for strength improvement. We proposed fiber-looped deltoid structure as shown in figure 22. In this structure, fiber layers are added to the deltoid side of the L-shaped parts, leading to higher bending stiffness. Therefore, the lateral deformation can be suppressed by using this structure. We conducted tensile tests using asymmetric laminate design, fiber-looped deltoid, and hybrid structure, which combined each of them. Digital Image correlation (DIC) was also carried out to measure cross-sectional strain distribution. In asymmetric laminate design, initial failure load and maximum load were enhanced compared to the symmetric laminate, showing that suppression of residual deformation leads to strength improvement. From the DIC tests, it was confirmed that lateral deformation was restrained by using the fiber-looped deltoid. As a result, initial failure load was improved by 13.8%, showing the effectiveness of the structure. Hybrid structure reduced spring-in deformation and enhanced both initial failure load and maximum load. Especially in maximum load, 24.9% improvement was achieved compared to the symmetric specimen.

3.6 Effect of taper angles on delamination strength of tapered composite laminates

Yuichiro Aoki, Sunao Sugimoto, Yutaka Iwahori and Toshiya Nakamura
Japan Aerospace Exploration Agency, Japan

In the design of composite airframe structure, a tapered section is generally used to achieve optimum weight reduction of a structure. The laminate thickness needs to be tailored according to local loads distribution, but in composite structures, thickness change cannot be achieved in a continuous way like metallic structures. In practice, tapering in laminate thickness can be introduced by terminating plies at several locations. This is known as ply drop-off. Application of the ply drop-off is commonly used in current airframe structures like wing and empennage panels, helicopter rotor blades, etc. However, ply drop-off creates geometry and material discontinuities that act as sources for high inter-laminar stress concentration [1, 2]. Several studies have been carried out about damage initiation and delamination propagation in those ply drop-off areas [3-5]. These studies give basic ideas about the influence of ply drops on static and fatigue behaviors.

The objective of this study is to evaluate the effect of taper angles on damage initiation and delamination propagation. Additionally, the effect of the ply drop-off configurations is also investigated to improve the strength of tapered laminates avoiding or minimizing a critical damage.

The specimens are made from 0.19mm thick unidirectional prepreg tape with carbon fiber and epoxy resin systems. The number of plies varies from 16 plies at the thin section to 32 plies at the thick section. Geometry of the specimen is shown in Fig. 23(a). The layup is quasi-isotropic with fiber fraction of $[0^\circ / 90^\circ / \pm 45^\circ = 25\% / 25\% / 50\%]$. Three different types of tapered laminates are considered in this study shown as Fig. 23(b). Type 1 specimen has four different taper ratios of 1:5, 1:10, 1:20, 1:50. Type 2 and 3 specimens has different number of covering plies and ply drop configurations with a taper ratio of 1:20.

Tensile strength has been investigated under static load with 100kN hydraulic testing machine. The load was applied by displacement control at the rate of 1.0 mm/min. Table 1 shows the comparison of tensile strength for Type 1 specimens with different taper ratio, where the strength decreases with the taper angle increases. A stress concentration at the termination front of 0-degree layers caused an initiation of the matrix crack in a cover ply and subsequently that induces failure with delamination propagation. Table 2 shows the comparison of strength for Type 1, 2 and 3, where the strength and delamination propagation strongly depends on the ply-drop configurations.

Fatigue tests at a load ratio of $R=0.1$ also has been performed to evaluate delamination propagation after an initial damage. Fig. 24 shows the relationship between fatigue cycle and delamination length for Type 1,

where delamination propagation rate drastically increase with the taper angle increases.

Reference

- [1] Curry JM, Johnson ER, Starnes Jr. JH. Effect of dropped plies on the strength of graphite–epoxy laminates. *AIAA Journal*, 30 (1992) 449–56.
- [2] Kim JS, Rhee SY, Cho M, Simple and efficient interlaminar stress analysis of composite laminates with internal ply-drop, *Composite Structures*, 84 (2008) 73–86.
- [3] O. T. Thomsen, F. Mortensen, Y. Frostig, Interface failure at ply drops in CFRP/sandwich panels . *J. of Composite Materials*, 34 (2000) 135-157.
- [4] Steeves CA, Fleck NA, Compressive strength of composite laminates with terminated internal plies. *Composites: Part A* (2004) 1-8.
- [5] Ganesan R, Liu DY, Progressive failure and post-buckling response of tapered composite plates under uni-axial compression, *Composite Structures*, 82 (2007) 159-176.

3.7 Tokyo Metropolitan University - JAXA Collaborative Research on Composite Wing Structures

Hikaru Hoshi*, Naoyuki Watanabe**, Sunao Sugimoto*, Yutaka Iwahori*

Japan Aerospace Exploration Agency, Japan, Tokyo Metropolitan University, Japan*

The CFRP wing development study for a single aisle commercial aircraft is performed by JAXA and Tokyo Metropolitan University (TMU) under the TMU-Tokyo Metropolitan Government (TMG)-JAXA joint project, namely "Asian Human Resources Development in Aeronautics". Manufacturing and structural test of the Partial Composite Wing Structure (PCWS) program is one of our research project. Other research topic is design study of CFRP wing root joint structure.

A composite wing structure was designed to demonstrate the novel technology for the next generation single aisle transport aircraft. Our research target is assumed 150 seat class airliner which is same as the Boeing B737, and the Airbus A320. Two conceptual aircraft were planned for this project to conduct the design and manufacturing and test which are the 150 seats class of 6 abreast fuselage airliner. Figure 25 gives an image of 150 seat class airliner on this project. This conceptual aircraft was assumed that is widely used composite materials for wing, fuselage, and tail plane structure.

State of art materials and low cost / high speed manufacturing process are key technology to develop the next generation single aisle aircraft. New stitch composite with Vacuum assisted Resin Transfer Molding (VaRTM) Process, was prepared to meet this demand. Stitch composite has high impact resistance characteristics which derive from binding effect of thickness direction stitch thread. Therefore, VaRTM stitch composite was applied to the wing spar to eliminate the in-flight impact problem, complex shape drape problem, and cost. Spar splice is necessary for easy handling and manufacturing flexibility in wing assembly process. Electrical Heating Press Forming (EHPF) method was applied to titanium fitting of spar splice. This EHPF process is able to reduce the machining time and material cost due to near net shape forming by press machine process.

Structural test program of PCWS is configured strain survey, impact test, static test, fatigue test, and non-destructive inspection. This test program aims to demonstrate the new technologies and to extract the technical problems of practical uses. PCWS and test system are shown in Figure 26 and Figure 27.

KHI, TMU, JAXA has been work for a design study on the CFRP wing root joint structure. This CFRP wing root joint is conventional bolted design for composite skin/stringer structure. 6 configurations for the wing root joint were designed to compare each evaluation items. Evaluation items is composed the weight, maintainability, productivity and others. Each design types were selected from the I shaped skin/stringer, single lap shear, double lap shear, and various fittings. As result, double lap joint with two angle fittings was most efficient design, which composed the double lap titanium joint for skin and two titanium angle fittings for I shaped stringer.

Coupon and element tests were conducted by Building Block Approach (BBA), which include many coupon specimens and one subcomponent test. Over 260 coupon and element specimens were tested to establish the design allowable and the design value for initial design of bolted wing root joint. Finally, sub-component test article of upper wing root joint was tested to confirm the design ultimate load capability. Photo of BBA and sub-component test article are shown in Figure 28 and Figure 29.

3.8 Fatigue Test Trial of CFRP Coupon Specimens

Hisaya Katoh¹ and Toshio Ogasawara²

¹Japan Aerospace Exploration Agency, Japan

²Tokyo University of Agriculture and Technology, Japan

This report presents the fatigue life data of the CFRP quasi-isotropic laminate used in aircraft, acquired at JAXA and the results of the brief discussion on the handling of fatigue test data acquired by coupon tests. The fatigue tests conducted are tensile–tensile ($R = 0.1$), tensile–compressive ($R = -1$), open-hole compression ($R = 10$), and compression after impact ($R = 1.25, 2, 10$).

The prepreg used was a 180 °C cured-type unidirectional carbon fiber / epoxy composite material T800S/3900-2B from Toray Industries Inc. Using an autoclave, a laminated construction of $[45/0/-45/90]_{2S}$ (16 ply, 3 mm) and a laminate of $[45/0/-45/90]_{4S}$ (32 ply, 6 mm) were molded and used for the experiment. This material, called the inter-laminar reinforced CFRP, has excellent post-impact compressive strength characteristics for use in aircraft. The fiber volume fraction was 55% and the elastic modulus in the main axis direction was 49.2 GPa. The fatigue test conditions are summarized in Table 3.

In the tensile–tensile fatigue test, the relationship between the ultimate tensile strength and fracture lifetime is shown in Figure 30. The fatigue strength at 10^7 cycles was approximately 50% of the initial strength and a remarkable decrease in fatigue strength could be confirmed. Some cases were resistant to the tensile load and did not break even in a state where almost the entire surface was peeled off. Figure 30 shows the results when the ONSET of peeling progression is taken as the point at which the out-of-plane displacement exceeded 0.02 mm. The fact that delamination occurred from the initial stage of the fatigue test was confirmed again. In the tensile–compressive fatigue test, the fatigue strength at 10^7 cycles was approximately 50–55% of the initial strength.

Figure 31 shows the S-N diagram of the compression fatigue after impact. The slope of the S-N diagram tended to decrease with a decrease in the stress amplitude and the fatigue strength at 10^7 cycles for $R = 10$ was approximately 75% of the initial strength.

With these experimental results, we will briefly discuss the evaluation of the fatigue behavior of CFRP by coupon specimen. The fatigue strength at 10^7 cycles was approximately 50–55% of the initial strength in the non-hole specimen and approximately 75% in the open-hole specimen and the specimen imparted with impact damage. In the smooth coupon specimen, the impact of the progress of delamination from the edge portion was large and as a result, the fatigue strength decreased remarkably compared to the initial strength. On the other hand, compressive–compressive fatigue test on the open-hole specimen and the specimen after impact damage, where the impact of the peeling progression from the edge portion was less, resulted in a relatively smaller reduction in the fatigue strength. Since the structures of aircraft and automobiles generally have a significantly large area with respect to the edge portion, it is easy to imagine that the mode of fatigue fracture is largely different from the coupon test. Therefore, the fatigue strength as a structure may be considerably higher than the fatigue strength by coupon test. From this viewpoint, it is suggested the S-N diagram and the fatigue limit diagram of the CFRP laminate obtained by the coupon specimen are sometimes difficult to use directly in the design of the actual structure (actual life prediction). On the other hand, when the impact of hole circumference or impact damage is large, the impact of delamination from the edge portion is relatively small. Thus, considering just the dimensional effect, it is possible to acquire fatigue data, which could serve as a reference to some extent.

4 STRUCTURAL HEALTH MONITORING

4.1 Ultra-lightweight composite structures designed based on SHM and rapid repair system

Shu Minakuchi and Nobuo Takeda
The University of Tokyo, Japan

Carbon fiber reinforced plastic (CFRP) has remarkable mechanical properties and lightweightness. However accidental damage significantly degrades its strength, restricting design space of CFRP aircraft structures [1]. In this context, several structural health monitoring (SHM) technologies have been developed. If detected damage can be repaired immediately after its occurrence, CFRP structures can be designed to tolerate larger damage, and thus more lightweight and adaptable aircraft structures may be realized. This study proposes a new structural concept based on this idea (Fig. 32, [2, 3]). The thickness of the structure is significantly reduced for weight reduction and its structural health is checked after every flight using the integrated SHM system. If damage is detected, a rapid-cure composite patch is temporarily applied to the damage area before the next flight for safe operation during a certain period. In the next scheduled maintenance, the damage state is evaluated in detail using non-destructive inspection (NDI) and scarf repair is applied for the full strength recovery. The concept of this rapid repair is analogous to that of Quick Composite Repair (QCR) developed by Boeing [4]. A repair patch of non-heating curing composites (e.g., visible light cure composite) does not require a heavily equipped heater unit for consolidation, and thus damage can be repaired at the airport gate in a short time, which leads to minimal out-of-service time.

This study demonstrated the first ultra-lightweight CFRP panel designed based on the SHM and rapid repair system. First, the feasibility and technical merit of the new design concept was discussed along the lines with the current damage tolerance philosophy (Fig. 33, modified from CMH-17 [1]). If the thickness of the structure is reduced based on the new design concept, the strength curve moves downward in Quadrant 1 in Fig. 33. As a result the probability-of-failure curve also shifts downward, and a shorter inspection interval n is necessary for the safe operation. In the proposed concept (Fig. 34), the SHM system detects damage after every flight, and thus the safety requirement is sufficiently fulfilled. The rapid repair system then immediately recovers the strength with minimal downtime, and thus the continued safe operation is possible.

One of the key aspects to realization of this concept is the strength recovery by rapid repairing. If the recovered strength is higher than the ultimate load of the conventionally-designed structure (i.e., residual strength under the barely-visible-damage condition), the ultra-lightweight structure can be operated at least as safely as the conventional structure. So this project conducted compression after indentation tests of two composite stiffened panels based on the conventional and new design concepts. The thickness of the ultra-lightweight specimen was set to be half of the thickness of the standard specimen. First, the same quasi-static indentation displacement was applied to the stiffener flange position of the two specimens to introduce barely visible damage. Only the ultra-lightweight specimen was then repaired using a CFRP patch, which simulated rapid repairing after damage detection by SHM. Finally the two specimens were tested under compression. The conventionally-designed specimen failed at 40.5kN and the repaired ultra-lightweight specimen at 44.8kN (Fig. 34), successfully confirming that massive weight reduction is possible with the new design concept.

References

- [1] Composite Materials Handbook (CMH-17) vol.3, 2012, SAE International.
- [2] S. Minakuchi, M. Takai, H. Otake, and N. Takeda, "Rapid repair concept for CFRP structures monitored by structural health monitoring systems: On uncertainty of detected-damage information," *Materials System*, 30, 47-51 (2012).
- [3] S. Minakuchi, K. Yokota, N. Takeda (2015). Ultra-lightweight Composite Stiffened Panel Designed Based on SHM and Rapid Repair System. *Structural Health Monitoring* 2015.
- [4] E. F. Walp, "Nick of time," *Frontiers*, 12 (9), 18-21 (2014).

4.2 Optical Fiber Sensor based Impact Detection System for Aircraft Structures

Akira Kuraishi¹, Yuji Ikeda¹, Hiroshi Mamizu¹, Keisuke Saito¹, Toshizo Wakayama¹,

Nobuo Takeda², Shu Minakuchi², Kiyoshi Enomoto³

¹ Aerospace Company, Kawasaki Heavy Industries, Ltd.,

² Graduate School of Frontier Sciences, The University of Tokyo,

³ R&D Institute of Metals and Composites for Future Industries(RIMCOF)

The application of composite materials to primary aircraft structure is contributing to the structural weight reduction. The challenge is that the composite structures are more susceptible to impact damages that can only be detected through detailed non-destructive inspection (NDI).

The authors have developed a structural health monitoring (SHM) system capable of detecting impact damages using the optical fiber sensors. The objective is to reduce the maintenance cost by focusing the time-consuming NDI on the regions of detected impacts. The system, shown in Figure 35, will be equipped on-board the aircraft and operated continuously during flight and ground operations. The FBG (Fiber Bragg Grating) sensors are ideal for constructing a light-weight sensor network over a wide area of aircraft structures.

The implementation of this technology is being studied through the JASTAC (Japan Airbus SHM Technology for Aircraft Composites) program, where potential use case scenarios are discussed and joint verification tests are performed. As a part of this program, the full-scale structure validation tests were performed in 2015 and 2016 jointly by Kawasaki and Airbus. The tests demonstrated the following capabilities of this technology.

- (a) Installation of the optical fiber sensor network on the actual aircraft structure.
- (b) Strain history measurement during fatigue loading simulating the operation loads.
- (c) Detection of impact with the sensor network bonded on the actual aircraft structure.
- (d) Durability of the sensor network under more than a year of fatigue loading.

Other applications tested and demonstrated by the authors are the following.

- (i) Detection of the blunt object impact (BOI) by a ground support equipment.
- (ii) Life cycle monitoring using the same embedded sensor network to monitor the composite part during the fabrication phase and the operation phase.

This work was conducted as a part of the project, "Advanced Materials & Process Development for Next-Generation Aircraft Structures" under the contract from the New Energy and Industrial Technology Development Organization (NEDO), founded by the Ministry of Economy, Trade and Industry (METI) of Japan.

4.3 Development of ultrasonic wave based structural health monitoring system for practical use

Hideki Soejima¹, Kohei Takahashi¹, Kensuke Yoshimura¹, Masakatsu Abe¹,
Megumi Hiraki¹, Nobuo Takeda², Noriyuki Sawai³

¹SUBARU CORPORATION, Japan

²University of Tokyo, Japan

³R&D Institute of Material and Composite for Future Industries (RIMCOF), Japan

The concept of Structural Health Monitoring (SHM) technologies comes from nervous system in living things. In a SHM technology, sensors are installed in aircraft structures to collect data which are analyzed to evaluate structural integrities automatically. SUBARU has been developing a SHM system, which can contribute to achieve the following results, for over ten years.

1. Reduction of maintenance costs can be achieved by using SHM system for inspections in maintenance actions.
2. Increase of aircraft availability can be achieved by using SHM system for inspections on accidental incidents in addition to periodical inspections.
3. Reduction of structural weight can be achieved by using SHM system for adopting novel design philosophies to the current design manners.

In the SHM system, shown in figure 36, Macro Fiber Composites (MFC) actuators oscillate ultrasonic Lamb waves which propagate in aircraft structures and Fiber Bragg Grating (FBG) optical fiber sensors detect the ultrasonic Lamb waves. The ultrasonic Lamb waves must change with the change of the structures, in which damages and/or defects are initiated and grown. The changes of the ultrasonic Lamb waves from that in intact condition are analyzed and evaluated by the SHM system; consequently, damage detection can be achieved and also structural integrities can be diagnosed by the SHM system. Several Ground tests have been carried out to verify probability of detection (PoD), environmental durabilities, and detection capabilities of the SHM system using from coupon specimens to full-scale test articles in order to fulfil requirements for applying the SHM system to actual aircraft. In addition to the Ground verification tests, flight verification tests have been conducted last year in order to evaluate two main subjects. Proof of concept on the SHM system was one of the subjects in the flight tests. Another one was to investigate the compatibility of the SHM system to an actual aircraft and to show that ultrasonic Lamb waves could be measured with the SHM system even during flights. The flying test bed (FTB), shown in figure 37, was used for the flight tests. Original aircraft of the FTB was Cessna Citation Sovereign and modified by Japan Aerospace eXploration Agency, JAXA. MFC actuators and FBG sensors were installed in the fuselage panel and the SHM interrogation unit were placed in the cabin with a rack. The flight tests were conducted in accordance with the planned flight patterns. Measurements of ultrasonic Lamb waves were conducted not only on the ground, but also during flights. Figure 38 shows the ultrasonic Lamb waves measured before and after the flight in hangar. The two ultrasonic Lamb waves are almost the same, which means that no change has happened in the portion of the fuselage panel. Namely, structural integrity of the portion monitored with the SHM system had been maintained after the flight as well, which showed that the concept on damage detection and structural integrities of the SHM system was demonstrated in actual aircraft operations. Some ultrasonic Lamb waves measured in flight, shown in figure 39, are almost the same as those measured in hangar. From the results shown in figure 38 and 39, ultrasonic Lamb waves have been measured successfully even during the flights with the SHM system. From the results, it was confirmed that the SHM system and the aircraft system were not affected each other and ultrasonic Lamb waves could be measured with the SHM system in the actual aircraft even during flights. From a result of these tests described here, it was confirmed that the technical maturity level of the SHM system had reached the level for actual uses. From now on, several verification tests with actual commercial aircraft will be conducted for practical use. In the future, the SHM system will be integrated with artificial intelligence in order to evaluate big data collected with not only the SHM system but also aircraft systems, which will make future air traffic more efficient and safer.

5 LIFE EVALUATION ANALYSIS

5.1 Application of Bayesian Method for Determining a Simple Reliability Index for Composite Material Strength

Seiichi Ito, Hisaya Katoh and Hikaru Hoshi
Japan Aerospace Exploration Agency

For the MIL-B basis as a binary statistical evaluation, at least 90% of the population of composite material strength is expected equal or exceed this tolerance bound with 95% confidence. This report integrates the reliability and confidence level, while building a reliability model of simple and unitary evaluation based on the Bayesian theory. The Bayesian method is applied to the uncertainty evaluation of unknown parameters to define the Bayesian expected reliability as a unitary reliability index for the allowable material strength. The construction of the Bayesian reliability method and a concrete evaluation example for the MIL-B value of the composite material strength are shown below.

The expected value of the reliability is defined as the Bayesian expected reliability. In the following, by assuming the uncertainty of the material strength is a normal distribution, the unitary reliability index is calculated. The material strength x of a normal population with mean μ and standard deviation σ is denoted by $N(x|\mu, \sigma^2)$. Describing the unknown parameter vector as $\theta = (\mu, \sigma^2)$, the Bayesian expected reliability $\underline{R}(x_a) = E[R(x_a)]$ at the allowable strength x_a is expressed by the following equation:

$$\underline{R}(x_a) = E[R(x_a)] = \int_{\theta} R(x_a | \theta) \cdot h^{(1)}(\theta | \mathbf{x}) d\theta \quad (1)$$

where $h^{(1)}(\theta | \mathbf{x})$ denotes the posterior joint probability density function (PDF) of the unknown parameter vector θ and $R(x_a | \theta)$ is the conditional reliability of θ at strength level x_a . The posterior joint PDF $h^{(1)}(\theta | \mathbf{x})$ is denoted as

$$h^{(1)}(\theta | \mathbf{x}) = \frac{P(\mathbf{x} | \theta) h^{(0)}(\theta)}{\int (Numerator) d\theta} \quad (2)$$

where $P(\mathbf{x} | \theta)$ determines the occurrence probability of the material strength data $\mathbf{x} = (x_1, \dots, x_n)$ conditional on the value of θ and n represents the number of samples. The prior PDF $h^{(0)}(\theta)$ indicates the degree of prior belief with unknown parameters θ , which can describes the engineering judgments and hypotheses about the parameters θ , before obtaining sample data.

In the Bayesian parameter estimation of the normal distribution, where the mean value μ and variance σ^2 are unknown, the non-informative prior PDF is used in both parameters where prior information cannot be introduced. Assuming that the standard non-informative prior $h^{(0)}(\mu, \sigma^2) \propto 1/\sigma^2$, then the posterior joint PDF $h^{(1)}(\mu, \sigma^2)$ in Eq. (2) is given by

$$h^{(1)}(\mu, \sigma^2) \propto \frac{1}{(\sigma^2)^{\frac{n}{2}+1}} \exp\left[-\frac{1}{2\sigma^2} \{S + n(\mu - \bar{x})^2\}\right] \quad (3)$$

where $S = \sum (x_i - \bar{x})^2$. This joint PDF has the ratio of a normal/inverse chi-square where the posterior of the μ conditional on the σ^2 is distributed as $N[\bar{x}, \sigma^2/n]$ and the marginal posterior of σ^2 is distributed as $S\chi_{n-1}^{-2}$ where χ_{n-1}^{-2} denotes an inverse chi-square distribution with $n-1$ degrees of freedom. Then, the Bayesian expected reliability, $\underline{R}(x_a)$, in Eq. (1) is calculated by applying Eq. (3).

First, $\underline{R}(n)$ in the Bayesian expected reliability in Eq. (1) when only the mean value is unknown is shown by the dotted line in Figure 40. As the number of sample n increases, the Bayesian expected reliability $\underline{R}(n)$ approaches a reliability level of 0.9. As an example of the sample size $n = 6$, the Bayesian expected reliability of $\underline{R}(n = 6) = 0.965$ corresponding to the MIL-B value can be seen in Figure 40. Next, the Bayesian expected reliability $\underline{R}(x_a)$ is shown for the MIL-B value where the mean and variance are unknown. As an example of the four types of composite material strength (A, B, C, D) shown in Table 4, the MIL-B value and Bayesian expected reliability of these materials are obtained and compared. From these results, the Bayesian expected reliability is $\underline{R}(x_a) = 0.996$ to 0.997 . In addition, the reliability index that is about 2 digits greater than the conventional binary evaluation corresponds to the MIL-B value $R=0.9$

The influence of the sample size n to the Bayesian expected reliability $\underline{R}(x_a)$ will be described next by using Material Data B in Table 4 as an example. Because there is no real sample data for each n other than $n = 6$, pseudo sample data with a different number of samples was created by the Monte Carlo method using the mean value and coefficient of variation of Material B. As n increases, the reliability index $\underline{R}(x_a)$ approaches $R = 0.9$, as indicated in Figure 40. This is an example showing the simplicity of the unitary reliability index by using the Bayesian expected reliability.

6 FULL SCALE TESTING

6.1 Structural Damage and Repair Assessment for MRJ Aircraft

Koji Setta, Toshiyasu Fukuoka, Keisuke Kumagai, Toshio Nakamura and Shunsuke Taba
Mitsubishi Aircraft Corporation, Mitsubishi Heavy Industries, Ltd.

Mitsubishi Aircraft Corporation and Mitsubishi Heavy Industries, Ltd. are developing and producing the next generation regional jet airplane as Part 25 airplane with 70-90 seat capacity. Structural design concept of MRJ is conventional except for the stabilizer structures composite material for which the new fabrication process of advanced vacuum assisted resin transfer molding (A-VaRTM) is applied [1]. Fuselage and wingbox are made of conventional aluminum alloys, such as 2000 series and 7000 series. Therefore, fatigue and damage tolerance characteristics will be the structural key drivers to achieve appropriate durability and operability.

Structural damage such as dents and lightning strike damage is likely to occur during the aircraft operations and will adversely affect dispatch reliability and increase down time. To reduce the maintenance cost and improve operational capability, preparation of sufficient ADL (Allowable Damage Limits) and standard repairs of SRM (Structure Repair Manual) will be required. Mitsubishi had numerous meetings with operators under the collaborative partnerships and set goals considering their field experience. ADL and repairs will be established by analyses supported by experimental testing with measurement technology. Substantiation approach considering building block is applicable. Fatigue and crack growth properties are justified by coupon or element level tests. Analysis methods are validated by element or subcomponent level tests. Full-scale fatigue test is also available if repairs are applied during test. (Figure 41)

For the evaluation of dent damage caused by the mechanical impact during operation, dynamic numerical analysis (LS-DYNA) and impact tests using the fuselage subcomponent structure were conducted to investigate the relationship between the dent size and the impact energy. During the impact tests, dent shapes are accurately scanned by the 3D measurement system (ARAMIS) and evaluated. As a result of this assessment, it is confirmed that the analysis methodology is useful to estimate impact energy from dent depth and vice versa as the virtual test. For example, it is useful to investigate the influence of impact energy, impact location and impactor shape. (Figure 42)

Doubler repairs likely generate new potential fatigue crack locations and are significantly affected by the selection of fastener type. Therefore, the effect of fastener type on fatigue strength and behaviour was investigated by the element level tests. The joint fatigue strength of blind rivet was lowest because clamping and hole filling effect were lower than solid rivets. Blind rivets are highly practical from the view point of accessibility and widely used, however appropriate operational limitation must be established considering fatigue and damage tolerance characteristics.

Durability of the typical damages and repairs are evaluated by the sub-component level tests. Multiple verification tests can be done in a short period by using Mitsubishi new designed fatigue test fixture which can simulate the cyclic pressurization for transport airplane fuselage. One of the key features of this test fixture is loading concept using negative pressure. Normally, this kind of pressure tests is conducted with the positive pressure applying to the internal side of fuselage, while this fixture uses negative pressure applying to the external side of fuselage. This enables to go forward with the test quickly and also prevent injury from dangerous bursting during the test [2]. Furthermore, longitudinal loading can be simulated in addition to pressurization load as necessary. (Figure 43)

References

- [1] Komori, Y., Takeda, F., Shono, T. In: A-VaRTM Technology Application on Primary Aircraft Structures, Proceedings of the 10th International Conference, SAMPE Japan.
- [2] Tsukigase, K., Fukuoka, T., Kumagai, K., Nakamura, T., Taba, S. In: Curved Panel Fatigue Test for MRJ-200 Pressurized Cabin Structure, Proceedings of the 28th ICAF Symposium, Helsinki, 3–5 June 2015, pp. 276–286.

6.2 Full Scale Strength Tests of XP-1 Aircraft

Yasuhiro Kanno and Toshimitsu Hayashi

Air Systems Research Center, Acquisition Technology and Logistics Agency (ATLA), Japan

Since 2001, Japan Ministry of Defense, Technical Research and Development Institute (currently ATLA) has been conducting a simultaneous development of the next-generation maritime patrol aircraft (XP-1) which is the successor to P-3C operated by the Japan Maritime Self-Defense Force and the next-generation cargo transport (XC-2) which is the successor to C-1 operated by the Japan Air Self-Defense Force. The development of XP-1 completed in March, 2013.

The structural integrity of XP-1 was verified by three full scale strength tests which were the static test (included 12 load conditions for rigidity, 71 load conditions for limit load, and 72 load conditions for ultimate load), the durability test under spectrum loading equivalent to 2 design service lifetimes, and the damage tolerance test under spectrum loading equivalent to 2 design service lifetimes with initial cracks at 38 locations followed by the residual strength test (3 load conditions). Two full scale test articles delivered in 2006 and 2007 were used for these strength tests. One was for static test, and the other was for durability and damage tolerance tests.

In 2013, TRDI successfully completed the strength tests for the XP-1, validating the static and fatigue strength of the primary structure and acquiring the technical data on damage tolerance to cover the aircraft's full design service life.

6.3 Full Scale Strength Tests of XC-2 Aircraft

Yasuhiro Kanno and Toshimitsu Hayashi

Air Systems Research Center, Acquisition Technology and Logistics Agency (ATLA), Japan

In 2001 the Japan Ministry of Defense launched the next-generation cargo aircraft (XC-2) program together with the next-generation maritime patrol aircraft (XP-1) program. The significant challenges in the structural design of XC-2 came from the performance and operation requirements which included three times longer range flights at higher cruise altitude and faster speed ($\geq 0.8M$) with three times larger payload capacity than C-1 aircraft currently operated by the Japan Air Self Defense Force (JASDF) in order to enhance effective international missions via commercial air corridors. Accordingly, the XC-2 was designed to be the largest cargo aircraft that Japan has ever built, equipped with a high-wing, a T-tail, twin turbofan engines (General Electric CF6-80C2) and rear loading cargo/ramp doors (figure 45).

The development of the XC-2 airframe structure was based on a building block approach, the final phase of which required full-scale static and fatigue testing to validate analysis. The full-scale static test involved a complete airframe test as well as a number of full-scale component test (e.g. flap, stabilizer, etc.) for static strength. On the other hand, the aim of the full-scale fatigue test (FSFT) was to demonstrate and validate the fatigue and damage tolerance behavior of the aircraft. The FSFT program has been re-planned recently to finish by FY2022 so as to evaluate the C-2 production airframe which includes redesigned structures based on the findings from the full-scale static test. The following will discuss the full-scale static test which has completed in 2016 since it covered the majority of the primary structure in this program.

The XC-2 full-scale static test (FSST) program was comprised of 70 load conditions including flight conditions (e.g. symmetrical/unsymmetrical maneuvers, steady/abrupt maneuvers, gusts, engine failure, pressurization, etc.), ground handling/landing conditions (e.g. braking, pivoting, turning, drift landing, etc.) and other miscellaneous conditions. They were selected from hundreds of the design load conditions based on the following criteria: a) the highest external/interface load conditions which are encountered in the flight envelop, b) the critical load conditions with respect to strength margin, c) load conditions required (or recommended) by civil/military regulations. The validity of the design loads was demonstrated by the flight load survey program with the instrumented aircraft during roughly the same period as the FSST.

The FSST article was composed of the fuselage, wing, engine pylon, vertical/horizontal stabilizer, nose/main landing gears and loading cargo/ramp doors (figure 46). The test loads were applied to the article in order to simulate design loads such as aerodynamic loads, inertial loads and internal pressure using a variety of discrete loading fixtures and hydraulic actuators. Prior to actual loadings, an aircraft-level finite element analysis was done to ensure that the appropriate test loads were utilized (figure 47). Extensive amount of bonded tension pads covered almost the entire surface of wing/stabilizer where out-of-plane load bearing structures (e.g. stringer, rib, etc.) were available on the back-side. The fuselage shell was loaded with bonded shear pads for inertial load as well as loading fixtures attached inside to apply loads directly to the cargo floor. The exterior of the aft-fuselage was loosely wrapped with protective textile straps to mitigate the risk associated with an unlikely burst during cabin pressure tests using pressurized air. Approximately 100 hydraulic actuators for each load condition were tied to whiffle-trees for the distributed loads or structural hard points for direct input of test loads. As each test is conducted, 7,500 sensors of strain and displacement measurements at the maximum were taken to monitor major load paths and local stress/strain at critical points in which strength margin were small.

The overall development and qualification of the XC-2 static strength successfully met the challenging design requirements via analysis and structural design changes, whereas it suggested wide range of topics to be tackled. Some of the topics were traditional elastic instability and large deformation problems under compression, such as buckling of a wing spar coupled with another buckling of an adjacent wing skin, lateral-torsional buckling of a tall and thin-walled frame in an aft-fuselage with oval cross-section under pressurization, and so on. They required complex and time-consuming adjustment to boundary conditions, mesh setting, element selection even using up-to-date finite element analysis with geometric and material nonlinear models in order to avoid unexpected failures.

6.4 Full Scale Static Test of X-2 Advanced Technology Demonstrator

Yasuhiro Kanno and Toshimitsu Hayashi

Air Systems Research Center, Acquisition Technology and Logistics Agency (ATLA), Japan

The Advanced Technology Demonstrator (X-2) is an experimental aircraft designed for evaluating the maturity and integration of advanced engine and airframe technologies for future fighters (figure 48). The single-seat X-2 is powered by ATLA/IHI XF5-1 engines with a thrust vectoring control system which consists of three paddles per engine at the rear of the fuselage to provide higher maneuverability. The airframe features stealth-oriented configuration such as parallel alignment of outer edges and serrated skin joints to return a narrower radar signal in a limited direction. This project was started in 2009. The X-2 is currently undergoing a variety of flight tests since its successful maiden flight on April 22nd, 2016.

As one of the requirements for strength flight release, full-scale static test and several full-scale component tests were successfully completed in January 2016 by the ATLA test team in close cooperation with Mitsubishi Heavy Industries, Ltd which is the prime contractor for the X-2 project. The full-scale static test program consisted of two separate test rigs. One was a main test rig for an almost complete airframe including fuselage, wing and vertical stabilizer, the other one was for the horizontal stabilizer only. Figure 49 shows the configuration of the test rig and setup. The representative 32 load conditions were applied to the full-scale test article using up to 40 hydraulic actuators, whiffle trees, load introduction fittings and dummy structures. Approximately 2,500 sensors were utilized to record strains and deflections during the test. The airframe exhibited sufficient static strength for ultimate loads through the ultimate load static testing and validated structural analyses with environmentally compensated reduction in strength for composite structures.

7. MISCELLANEOUS

7.1 An amphibian and the concept of its derivative model for firefighting application

Katsuo Tanaka, Atsuhiko Fujitani, Yushi Goda, Masatoshi Tsujii
ShinMaywa Industries, Ltd., Japan

The concept of firefighting application for US-2 (Fig.50)

The US-2 is the search and rescue amphibian that is being operated in Japan Maritime Self-Defense Force. Against the backdrop of the fact that seaplanes are being used for aerial firefighting operation in some foreign nations, the study to convert the US-2 for this application is ongoing. To enable releasing water in the air to extinguish fires, the fuel tank in the fuselage is planned to be converted into the water tank with the additional door provided at the bottom of hull to drop the water. The US-2 Firefighting Amphibian would be the unrivaled firefighting aircraft that can carry about 15 tons of water and deliver it while cruising at extremely low speeds.

The study of structural strength

Tests mainly for performance and functionality like the flight simulation test or the water dropping test with the actual-size mock-up of water tank (Fig.51) had been conducted as the study for realization of firefighting application. The study of effect on structure strength by conversion to firefighting application should be conducted hereafter. We are making study of specific loads for firefighting and plan to make study of fatigue strength including these loads.

7.2 Visualization of strain distribution and portent of destruction in structural material through mechanoluminescence

Nao Terasaki¹, Yuki Fujio¹ and Yoshitaro Sakata¹

¹ National Institute of Advanced Industrial Science and Technology (AIST), 807-1 Shuku-machi, Tosu, Saga 841-0052, Japan, nao-terasaki@aist.go.jp

Mechanoluminescent material is a novel functional ceramic powder (size: 10 nm—100 μ m, representative and the most efficient ML material: $\text{SrAl}_2\text{O}_4:\text{Eu}^{2+}$) and it can emit intensive light repeatedly accompanied by mechanical stress such as deformation, friction, impact, even in elastic deformation region. The ML intensity is proportional to Mises strain energy of the material. Thus, when dispersedly coated onto a structure, each particle acts as a sensitive mechanical sensor, while the two-dimensional (2D) emission pattern of the whole assembly reflects the dynamical strain/stress distribution inside the structure (Fig. 52) and the mechanical information around defect and crack or the invisible tip.

Meanwhile, in the field of a next-generation automotive and aerospace, multi-material concept has been rapidly accelerated, in which various kinds of material such as high-tensile strengthen steel, aluminum (Al), titanium (Ti) and carbon fiber reinforced plastic (CFRP) are used at the same time at appropriate position for each purpose. Actually, CFRP and other composite material are intentionally used in airplanes in high ratio (50 % for Boring 787, and 53 % for airbus A350 XWB) and automotive car not only in a concept car and a racing car but also in a popular car such as BMW i-3/8 from the viewpoint of light weight vehicle and energy saving. Therefore, here, we introduce results of ML visualization of (1) a strain contribution on CFRP in Fig. 53 and (2) real-time monitoring of transverse crack inside of CFRP in Fig. 54.

In Fig. 53, the strain distributions on twill woven CFRP are visualized through ML patterns during load application in tension and torsion. In the case of tension, the ML pattern shows almost same as the pattern of the original twill woven of CFRP, and the brighter area was respond to the area in which the direction of the fiber was same as the one of loading. This indicated that the stress was mainly contributed to the area with same fiber direction as loading. On the other hand, in the case of torsion, the load can be expected to be contributed to entire area with both fiber directions, and actually mechanoluminescence was observed from entire area.

The failure process of CFRP laminates involves not only fiber breakage but also microscopic damage such as transverse cracks and delaminations. Especially, transverse cracks in off-axis plies occur at much lower stress than the ultimate tensile strength of the laminates. Because it is important to detect the occurrence of the transverse cracks as portent of CFRP destruction in real time for reliability in use, the occurrence of transverse crack has been investigated using ML sensing. The CFRP composites specimen was provided from prof. N. Takeda and the laminate configuration was cross-ply $[0_2/90_4/0_2]$. From the preliminary experiments, the first transvers crack was generated at round 0.8 % strain (8000 μst).

At the low strain range such as 0–0.3% strain (3000 μst), mechanoluminescence was observed from entire area without specific pattern accompanied by tensional load and this indicates there is no crack generation in this stage as shown in Fig. 54(b). On the other hand, from around 0.8 % strain, specific straight ML patterns were gradually recording in perpendicular direction to the tensional loading. After the specific ML emissions, the ML specimen was unloaded immediately and entire cross section of the CFRP specimen was observed carefully using digital microscope. As the result, only at the responding positions to ML emissions, transverse cracks were confirmed in the cross-sectional microscopic image, as shown in Fig. 54(d). This clearly shows the usefulness of ML sensing for real time monitoring transvers crack occurrence in both of position and timing.

7.3 Development of Analysis and Test Methods for Lightning Strike on CFRP structures

- Current Density Analysis : Takayuki NISHI, Hiroyuki TSUBATA , Yasunori SATO (SUBARU)
- Spark Detection Technology : Shinya Ohtsuka (Kyushu Institute of Technology)
- Multi-Layer Current Density Analysis : Yoshihiro BABA (Doshisha University)

In recent years, due to frequent use of CFRP materials for the structure of aircraft, lightning protection technology has been developed as an important issue of aircraft design. In particularly, lightning current is complicated due to the effect of anisotropy by carbon fiber of CFRP, causing thermal damage and fuel ignition by spark in unexpected current concentrates. So this reason, new lightning protection design is urgently required. In order to develop more affordable and rational design tools, lightning current density analysis which can simulate fiber dominate phenomena for CFRP material and more efficient ignitable spark detection technology have been developed.

However, it is difficult to predict the accurate current distribution of fiber dominate phenomena by conventional current density analysis method. Therefore, a new numerical modeling technique of FDTD, which combine Triangular Prism Cells (TPC) into the shape of a square and an octagon for building up the fiber anisotropy to a grid, has been developed. This modeling technique has been able to analyze not only in each layer direction but also in the thickness direction, contacts with different materials and in complex structure shape. Figure 55 shows an example of current density analysis of a fastener-jointed CFRP panels by developed TPC modeling. The new analysis method could analyze not only the current density on each CFRP layer but also the current concentration around the fastener jointing portion.

The ignitable spark detection technology using optical fiber and photo-multiplier tube has been developed. Figure 56 shows the effectiveness of ignitable spark detection technology. This new technology has a higher accuracy and more efficient process than a conventional method that is by human determination using a digital camera.

Applying the new current density analysis method for the lightning protection design and the efficient ignitable spark detection technology will make the design of composite structures more accurate and efficient in the future.

7.4 INTRODUCTION OF EFFORT ABOUT CONSTRUCTION FOR FRACTOGRAPHY DATABASE IN JAPAN

Kenta Yamagiwa

National Institute for Occupational Safety and Health, Japan, 1-4-6, Umezono, Kiyose, Tokyo, Japan

Abstract: Fractography is performed in the process of failure analysis. However two problems were pointed out. One is that its result is qualitative. Nowadays, fracture surface is analyzed by skilled persons. They observe the surface, and suppose fracture mechanics, cause of accident and so on. Therefore, the result depends on the observer's skill. If the observer misunderstands the fracture surface, the adequate countermeasure for safety will not be lead. Next problem is age of skilled person. Especially in Japan, they are aged and going to retire. However, young and non-skilled person has not inherited their skill and knowledge. To solve these problems, the image database of fracture surface, which is called as "fractography database", is considered to be effective. In Japan, the committee to collect the fracture surface and other related data, i.e. experimental data and so on, is started to work from 2016. Here, the effort to collect the data is introduced.

1. Introduction

Since fracture processes remain on fracture surfaces, fractography methods are usually applied to failure analysis of actual components. In Japan, it becomes serious problem that aging skilled operators of fractography retire without handing down their techniques to next generation. Because number of engineers for failure analysis is decreasing, and many experiences and high technique of analysis are needed to investigate the fracture mechanics from fracture surfaces correctly. Moreover, result obtained only by observation depends on analyst's experience. Therefore, especially for result obtained by beginner's analysis, it remains lack of objectivity.

In order to solve these problems, it is considered that quantitative parameters, which characterize fracture surface, should be introduced to fractography. In this paper, therefore, we developed a fracture surface database system which can be easily used on the Internet to support unskilled engineers to analyze fracture surfaces.

2. System and data configuration of fractography database

2.1 System

The database is currently on the web server with the Wikipedia's source code. Users can easily access thorough the Internet by using the web browser. Temporally, the URL is <http://yamagiwa.org/fract-wiki/>. Users can search by some keywords and read the appropriate data as the data sheet. Figure 57 is the example of data sheet.

2.2 Configuration of data table

There are two types of data in the database. One is the text data to hold the attribution of fracture surface. For example, they are "material name", "fracture surface obtained by the experiment or by the actual equipment", "environment", "observer's comment" and so on. The other is the image data of fracture surface with the magnification and the width and height size of the image. The details of data configuration are shown in Table 5.

Especially, the "observer's comment" is considered to be important to preserve the skilled engineer's knowledge. The beginner observer can read and learn what the skilled persons looked and how they understood fracture surfaces.

2.3 Data collection

JSMS Committee on Fractography organized a small committee for database with JSMS Committee on Fatigue in 2016. In the committee, the configuration of data table and the fracture test to obtain the fracture surface for this database are discussed. In 2017, the specimens of carbon steel, stainless steel and aluminum for fatigue, tensile and charpy impact test will be performed at some universities and testing companies. It will be listed in the early 2018.

Data is not only collected by the experiment but also from the published papers, the past experimental works and the reports of accident investigations. Especially, data from the actual equipment accident is important and worth to learn. However, this kind of data is usually classified. Data collection about actual equipment is still being discussed in the small committee.

3. Conclusions

Here, fractography database is introduced and the effort of JSMS's committee for the data-base is also reported. It is considered to help the beginner observer's for fracture surface.

Acknowledgements

The authors would like to acknowledge the financial support of the National Institute for Occupational Safety and Health, Japan (JNIOSH) and Japan Society of Material Science (JSMS).

7.5 AIRCRAFT ACCIDENT INVESTIGATION

Aircraft Accident and Serious Incident Investigation

Kazuhiko Hirai

Japan Transport Safety Board (JTSB)

(1) Total number of registered aircraft in Japan

As of December 31, 2016, the number of registered civil aircraft in Japan was 2,767, consisting of 1,306 airplanes (of which 614 airplanes with jet engines), 811 helicopters, 650 gliders inclusive of motor gliders and one airship.

(2) Statistics related to the accident and serious incidents investigation

The number of accidents and serious incidents which JTSB investigated in the past two years are shown in Tables 6 and 7. Of the total of 59 occurrences, large airplanes accidents and serious incidents were 15, small airplanes were 15 and rotorcraft were 12. Gliders, ULP (ultra light plane)s and others were remaining 17 occurrences.

(3) Fatigue failure related serious incident

1) Summary of the serious incident

On Sunday, July 8, 2012, at 16:56 (JST, UTC+9hrs), a McDonnell Douglas MD900 rotorcraft started to take off from the landing field on the roof of an Hospital to transport an emergency patient from an landing field, with the PIC and three persons.

The rotorcraft, after going airborne, climbed for around 15 ft vertically while turning towards the direction of takeoff. As it started to move forwards from hovering, a low, hollow “boom” sound was heard from the left rear side, which was followed by the sound of the “ENG OUT” warning alarm. When the PIC looked at the instrument panel, the “ENG OUT” warning annunciator was flashing, and the tachometer (Np) and the torque meter for No. 1 Engine was displaying “0.” The tachometer (Np) for No. 2 Engine was within the green zone (normal area). However, the torque meter had indicated the red zone (no-excess range). Not to lose the altitude of Aircraft, the PIC increased the forward speed and avoided the obstacles without lowering the collective lever, and gradually increased altitude. The rotorcraft flew to another airport and landed at 17:09. Total time of usage of No. 1 Engine was 1,892 hrs and 6 min and total usage cycle was 8,217.

2) Extent of Damage to No. 1 Engine

The compressor turbine (CT) vane ring, CT blade, power turbine (PT) stator, PT blade, and turbine support case (TSC) were damaged. The CT blades and the PT blades were fractured around the full circumference and others were damaged by heat.

3) Inspections results of Engine

The CT vane ring had been severely damaged at the six o'clock position (viewed from the front) due to heat. One vane at the six o'clock position had been burnt away. Also, at the six o'clock position of the CT vane ring, there was evidence of remains of cracks across the outer wall of the CT vane ring.

Corrosion was also observed on the inner surface of the outer walls of the CT vane ring. Scanning electron microscope (SEM) analysis showed that the corrosion did not reach the parent material of the vane. Sulphidation was observed on the corroded surface.

Numerous axial small fatigue cracks were observed on the inner surface of the outer walls of the CT vane ring near the six o'clock position, which are thermal fatigue cracks. In addition, minor cracks were observed at the one o'clock and 11 o'clock positions of the CT vane ring. SEM analysis showed that the cracks near the six o'clock position of the CT vane ring extended from the inner surface to the outer surface, and cracks extended throughout the outer surface in the thinnest section of the outer wall. The cracks originated from the corrosion, but there were no evidence of sulfuric corrosion along the cracks. There were traces indicating

overheating near the six o'clock position of the CT vane ring, but no traces of overheating were found at either the one o'clock or 11 o'clock position.

4) Analysis of Findings

It is highly probable that the small axial cracks that had developed in the outer wall of the CT vane ring were thermal fatigue cracks that had developed due to being constantly exposed to high temperature on each flight. At the six o'clock position of the CT vane ring, there was evidence that axial cracks in the outer wall of the CT vane ring. It is probable that minor heat-fatigue axial cracks that were seen in other positions had also developed in the section of the CT vane ring (six o'clock position) that had been burnt away. Moreover, it is probable that the cracks that had developed at the six o'clock position had also penetrated the outer wall from the inside surface to the outside surface as with the cracks that had developed near the six o'clock position. It is probable that as the cracks penetrated the outer wall of the CT vane ring, the pressurized air from the exterior of the outer wall of the CT vane ring had entered the passageway of the combustion gas from the opening. It is probable that with pressurized air flowing into the high-temperature combustion gas, the oxidization of the section that had been penetrated by the cracks had accelerated. Also, it is probable that as the smooth flow of combustion gas was disturbed, the temperature distribution of the passageway of combustion gas was changed, and a localized increase in temperature had occurred. Due to this, it is somewhat likely that the corrosion due to heat for the CT vane ring at the six o'clock position had progressed further, and this also affected the cooling of the vanes, which further accelerated the corrosion of the vanes. As a result, it is probable that the CT vane ring at the six o'clock position had been severely damaged by the time of the occurrence of the serious incident. For the reason why the CT vane ring was severely damaged at the six o'clock position in comparison with the other positions, it is possible that the cracks that extended into the fillet radii of the vane and/or cracks that converged at a point had formed, and that this expedited the progression of the cracks. However, it was not possible to identify the cause of this as the CT vane ring had been burnt away.

ACKNOWLEDGEMENTS

The editors appreciated the members of the ICAF national committee of Japan Society for Aeronautical and Space Sciences and other participants in the committee, for their contribution in preparation of this national review and contributing discussion in the committee.

TABLES AND FIGURES

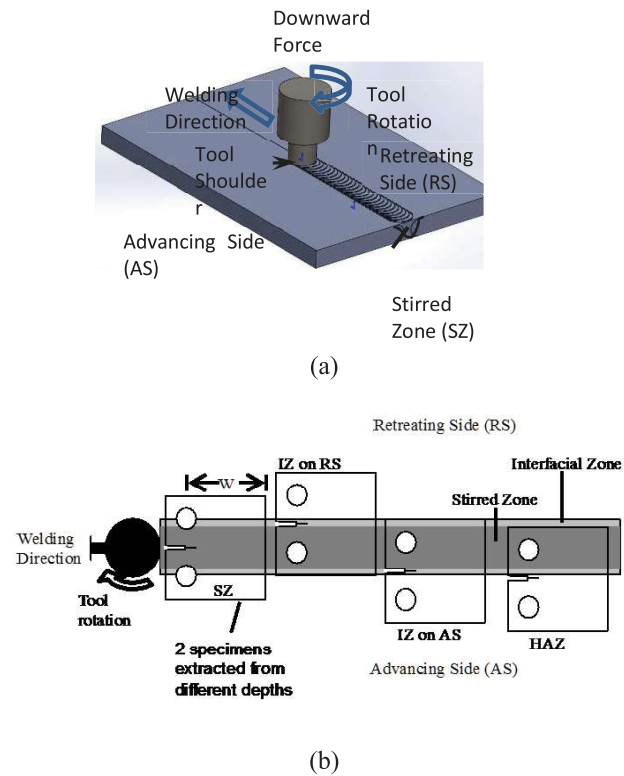


Figure 1 Miniature CT specimens extracted from the Ti-6Al-4V FSW joint.

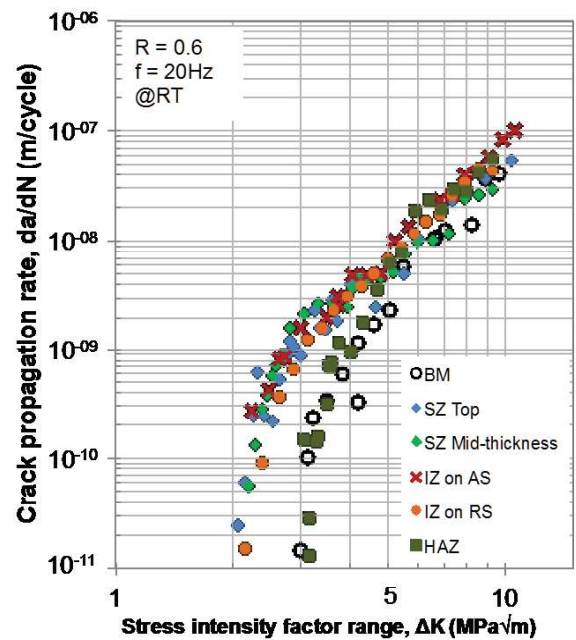


Figure 2 Fatigue crack propagation resistance dependent on the growing site in the FSW.

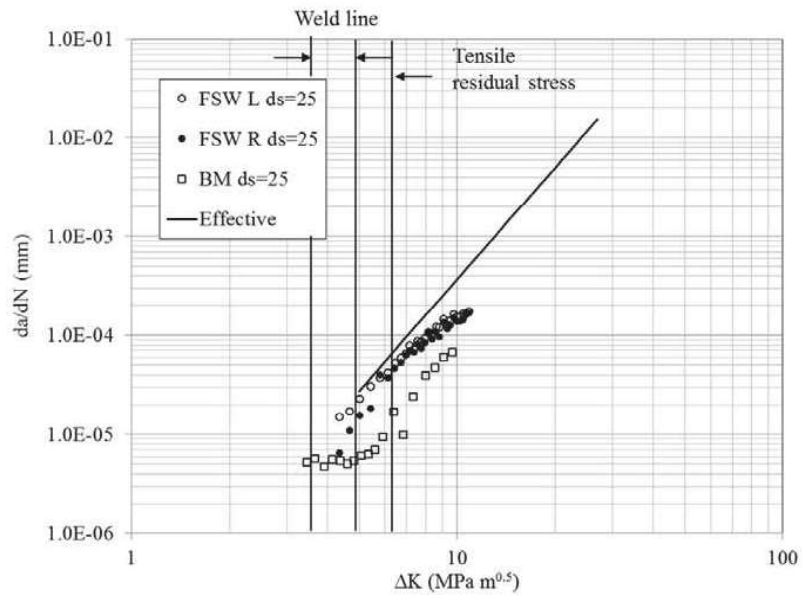


Figure 3 Fatigue crack growth rate of FSW joint ($\Delta\sigma = 25$ MPa)

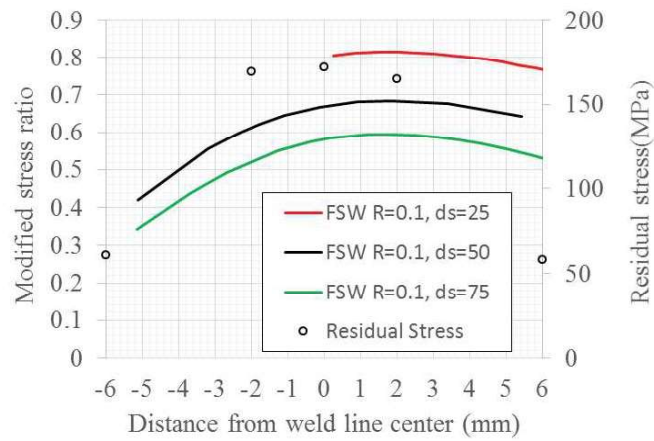


Figure 4 Variation of modified stress ratio to the location of crack tip

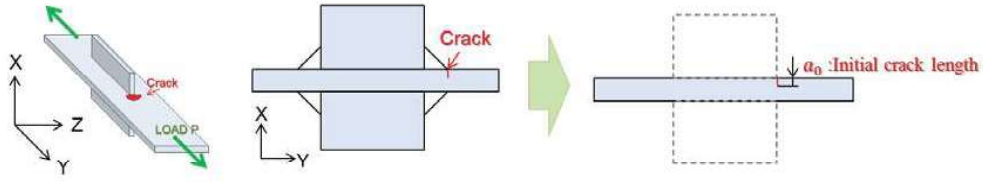


Figure 5 Basic scheme of equivalent crack length method

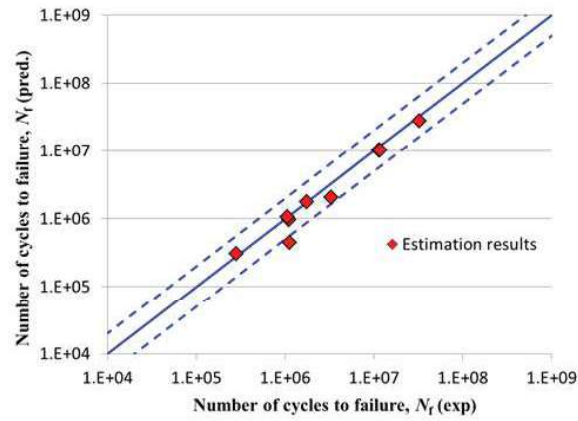


Figure 6 Estimation of fatigue life under step loading (Longitudinal gusset joints)

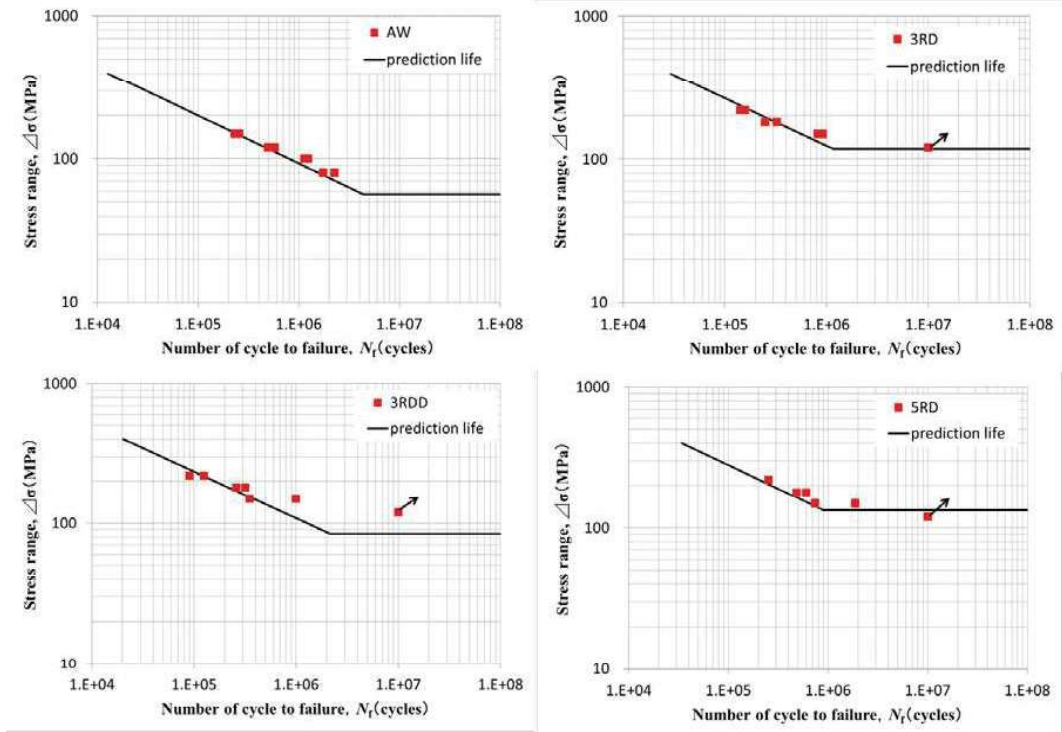


Figure 7 Estimation of S-N curves from K_t



Figure 8 (a) Geometries of hole notch cruciform specimen and (b) smooth cruciform specimen.

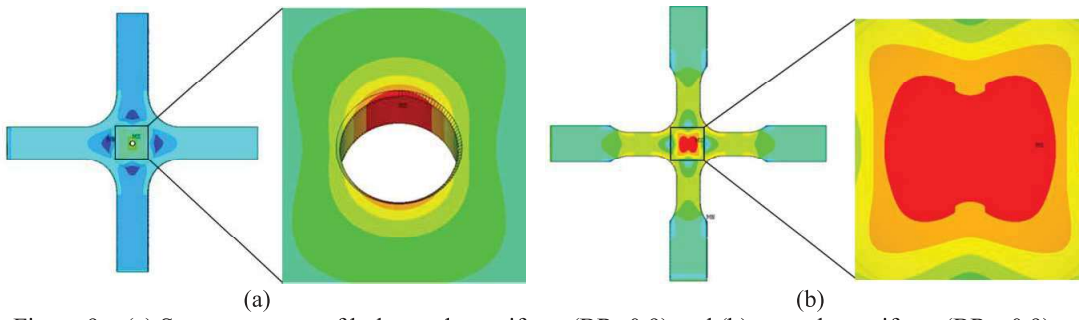


Figure 9 (a) Stress contours of hole notch cruciform (BR=0.9) and (b) smooth cruciform (BR=-0.9).

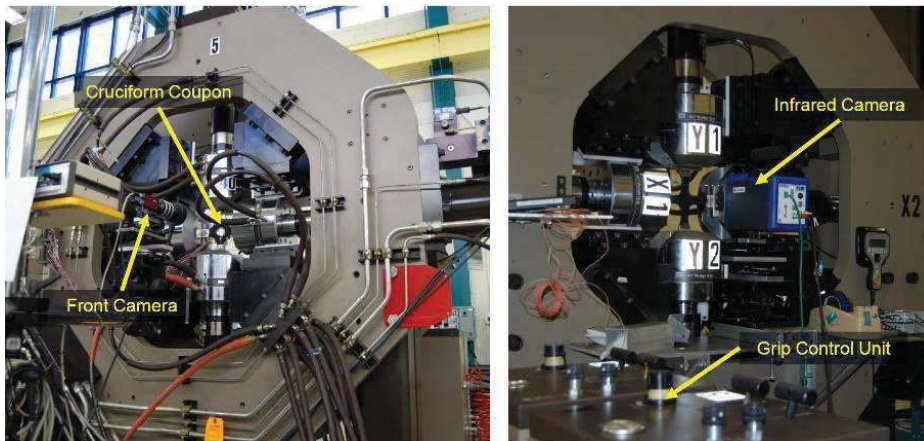


Figure 10 Biaxial testing machine in NRC.

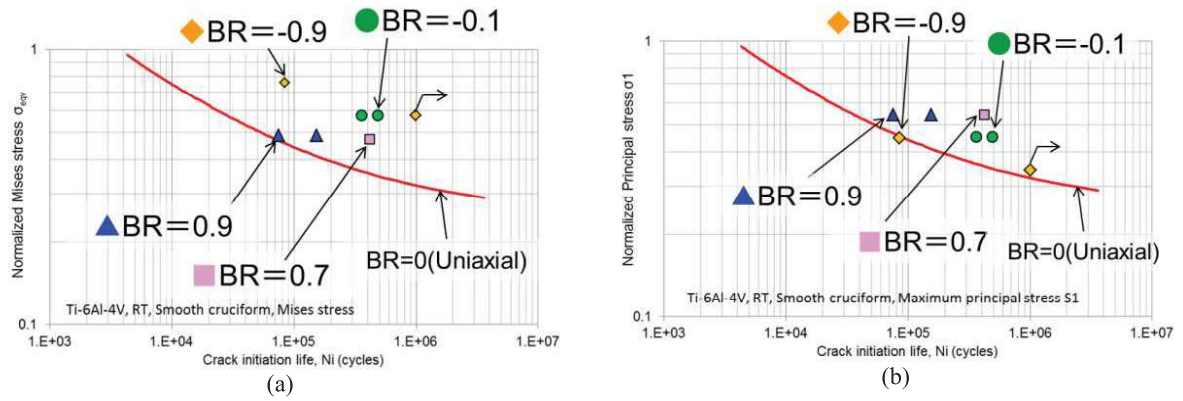


Figure 11 S-N diagrams of smooth cruciform specimen, life prediction using (a) the von Mises stress and (b) the maximum principal stress.

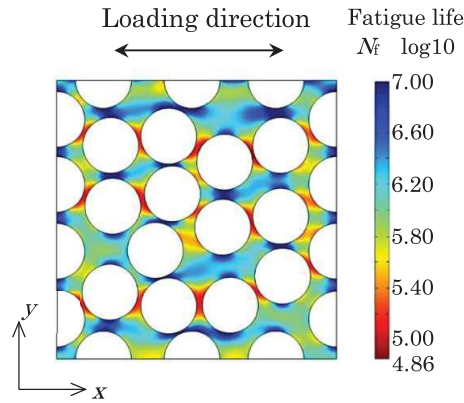


Figure 12 Fatigue life distribution in element model of the 90° unidirectional laminates applied maximum strain of $\varepsilon_{\max} = 0.5\%$.

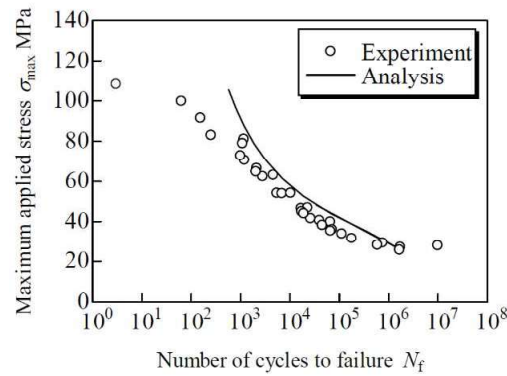


Figure 13 S-N diagram for the CFRTP 90° unidirectional laminates.

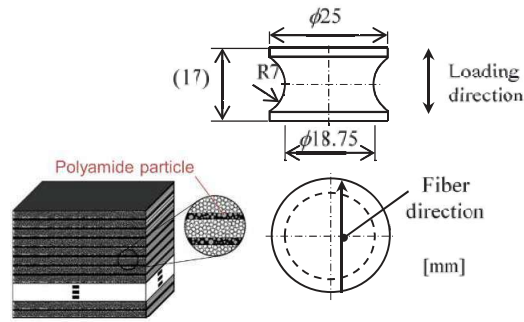


Figure 14 Schematic of thick CFRP laminates with toughened interlaminar layers and specimen geometry.

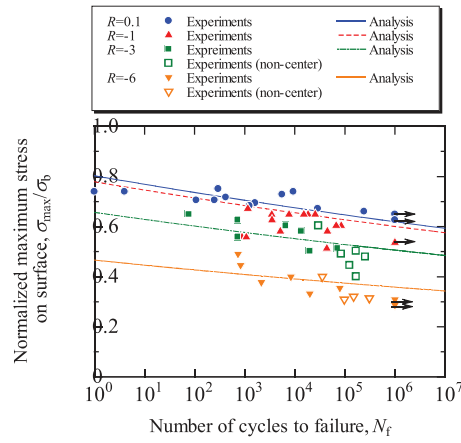


Figure 15 S-N curve of thick CFRP laminates in the out-of-plane direction at different stress ratios.

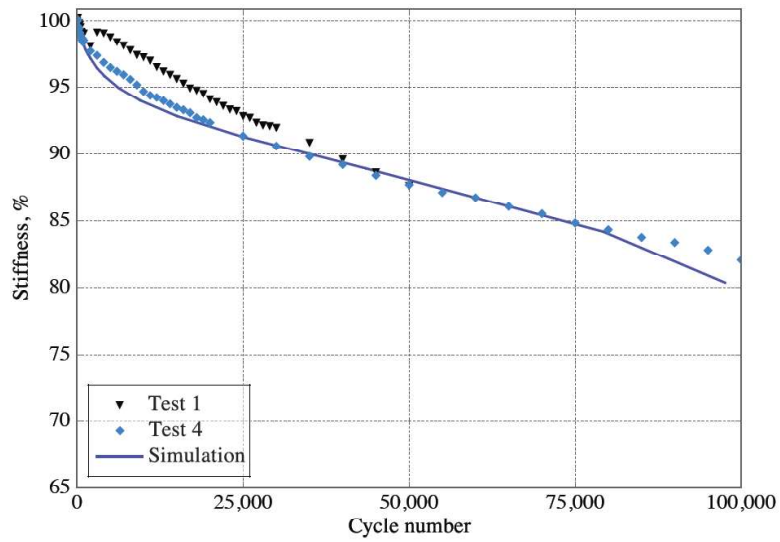


Figure 16 Stiffness degradation of $[\pm 45]_{ns}$ specimens during bending fatigue

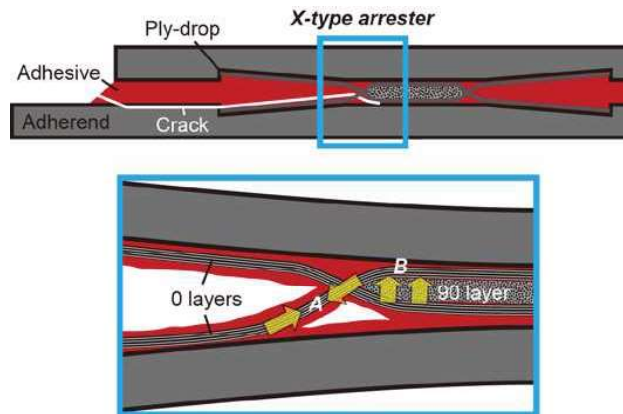
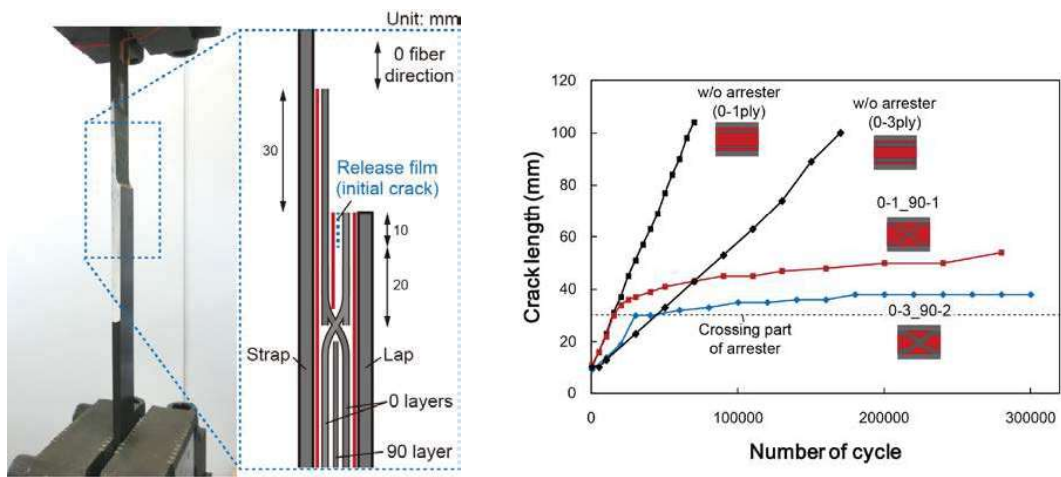


Figure 17 X-type arrester.



(a) Schematic of specimen.

(b) Fatigue crack growth curves obtained.

Figure 18 CLS fatigue test.

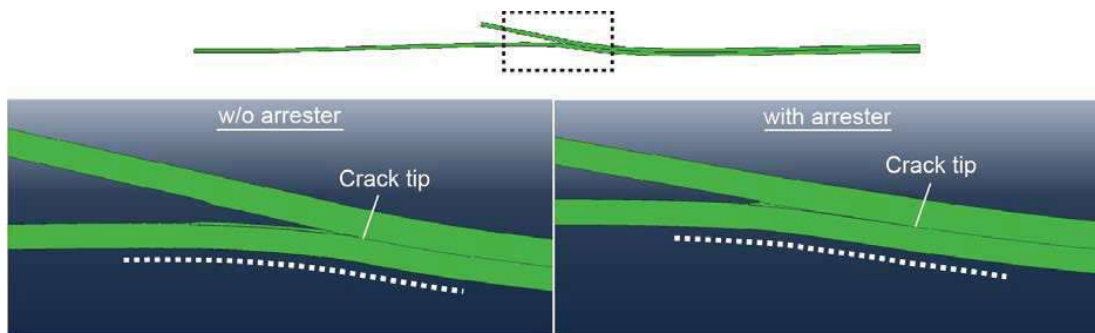


Figure 19 Deformation near crack tip. Arrester 90° layer constrained by 0° layers suppresses crack opening and secondary bending deformation, resulting in reduced energy release rate.

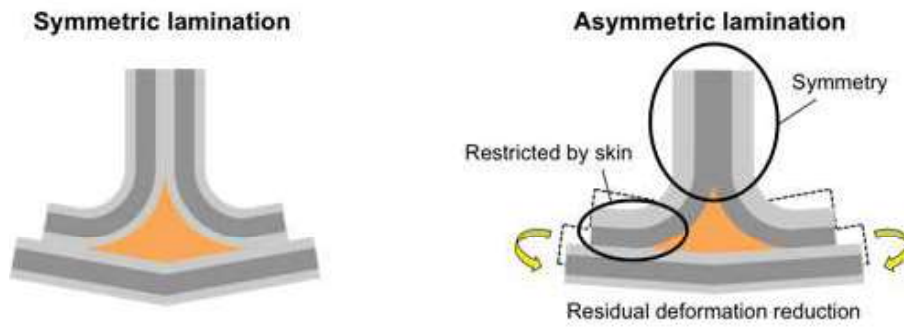


Figure 20 Design concept for reducing residual deformation without excess distortion proposed in this current study.

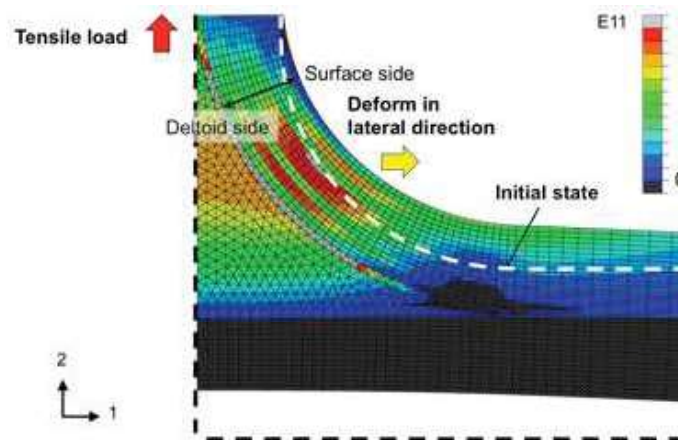


Figure 21 Lateral deformation under tensile load causing T-joint fracture.

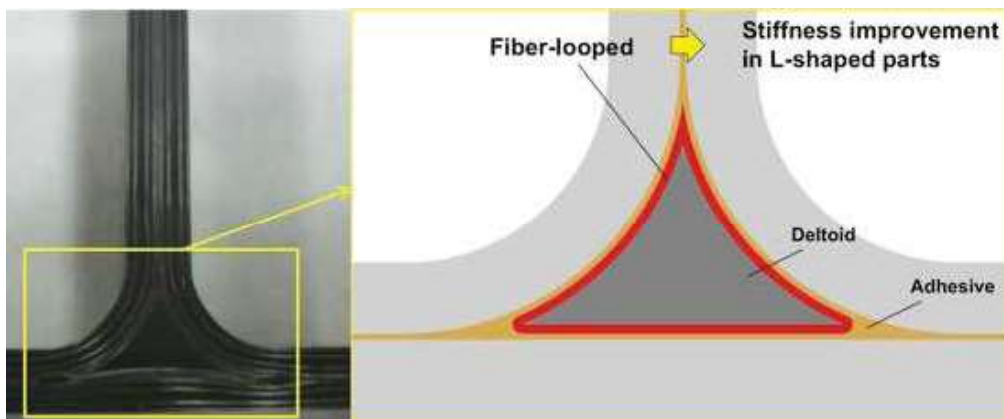


Figure 22 Schematic of fiber-looped deltoid structure.

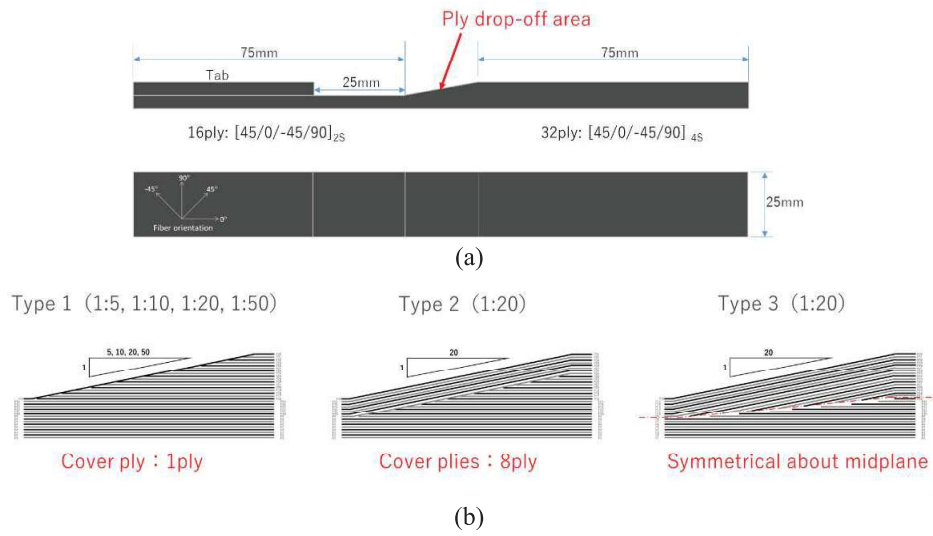


Figure 23 Test specimen, (a) geometry, (b) ply drop-off configurations

Table 1 Strength comparison for Type 1 specimens with different taper ratio

ID	Tensile strength [MPa] (Average value: n=3)		Shape
PDO5	<div></div>	441	
PDO10	<div></div>	527	
PDO20	<div></div>	605	
PDO50	<div></div>	824	
Reference*	<div></div>	908	

PDO~~X~~ means specimen with taper ratio of 1:~~X~~

*NHT strength for 16ply QISO laminates 2)T. Morimoto et al., JAXA-RM-14-004, p.171 (2014).

Table 2 Strength comparison for Type 1, 2 and 3 specimens with taper ratio of 1:20

ID	Tensile strength [MPa] (Average value: n=3)	
Type 1	<div></div>	605
Type 2	<div></div>	1017
Type 3	<div></div>	1018
Reference*	<div></div>	908

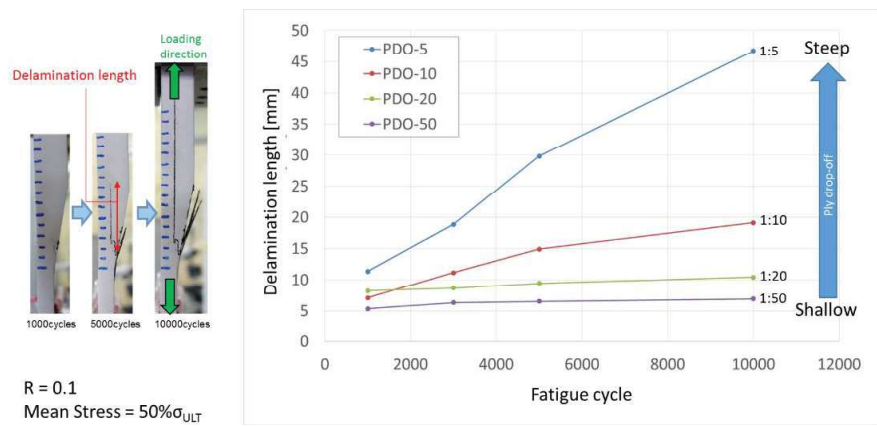


Figure 24 Relationship between fatigue cycle and delamination length for Type 1 specimens



Figure 25 Concept image of 150 seat class airliner.

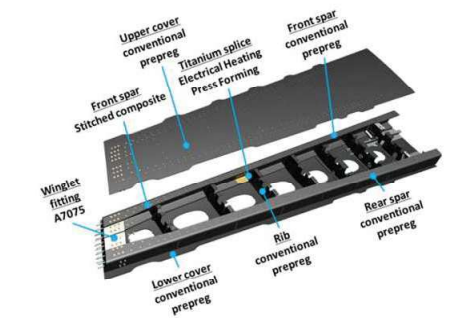


Figure 26 Partial composite wing structure

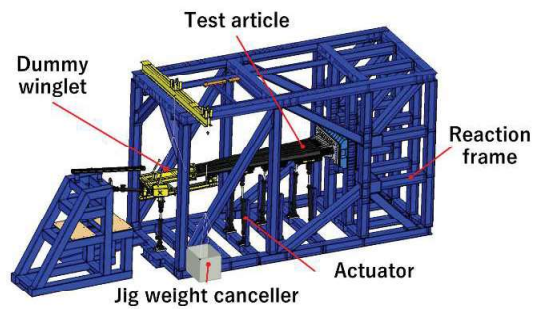


Figure 27 PCWS test system

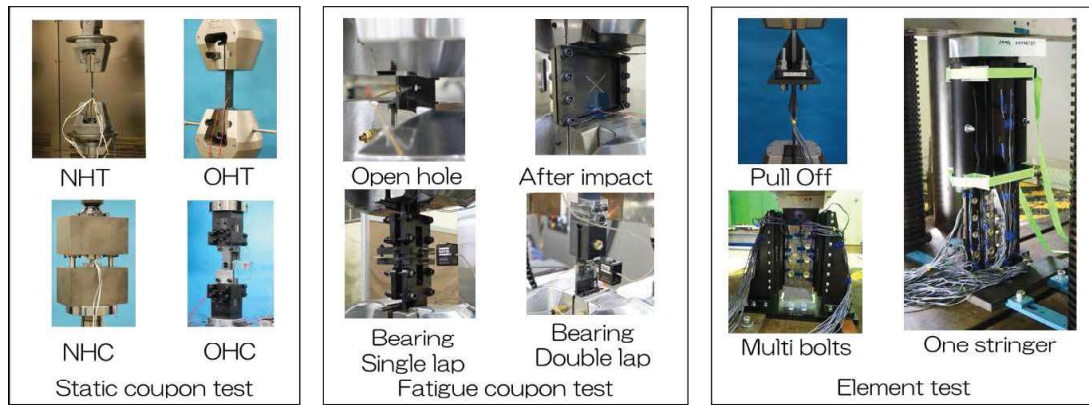


Figure 28 Building block approach for CFRP wing root joint structure



Figure 29 Test set-up of subcomponent test article

Table 3 Fatigue Test Conditions.

Fatigue Test	Fatigue Test Conditions
Tensile–Tensile (non-hole)	Frequency $f = 2$ Hz, Stress ratio $R = 0.1$ Truncation frequency 10^7 cycles, $N = 14$
Tensile–Compressive (non-hole)	Frequency $f = 5$ Hz, Stress ratio $R = -1$ Truncation frequency 10^7 cycles, $N = 14$
Compressive– Compressive (open-hole)	Frequency $f = 5$ Hz, Stress ratio $R = 10$ Truncation frequency 10^7 cycles, $N = 14$
Compressive– Compressive (after impact)	Frequency $f = 3$ Hz, Stress ratio $R = 1.25, 2, 10$ Truncation frequency 10^7 cycles, $N = 50$

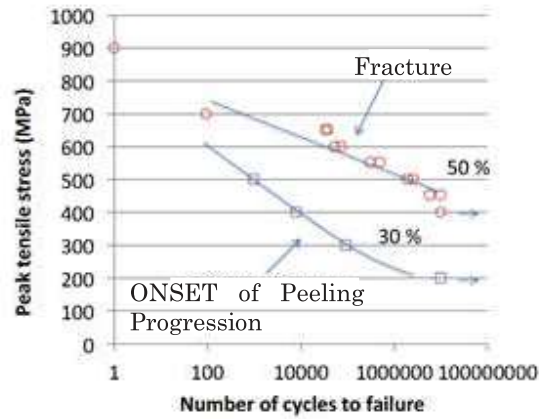


Figure 30 S-N Diagram (Non-hole, Tensile-Tensile Test, $R = 0.1$).

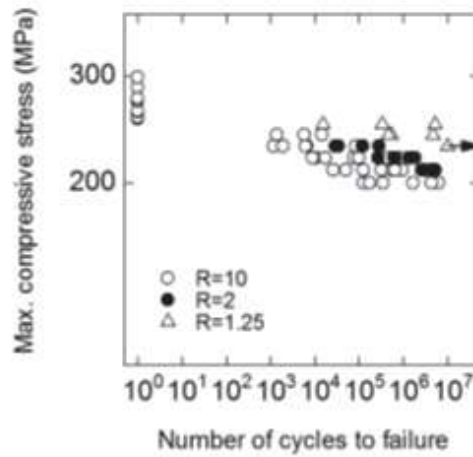


Figure 31 S-N Diagram (Compression after impact, Compressive-Compressive test).

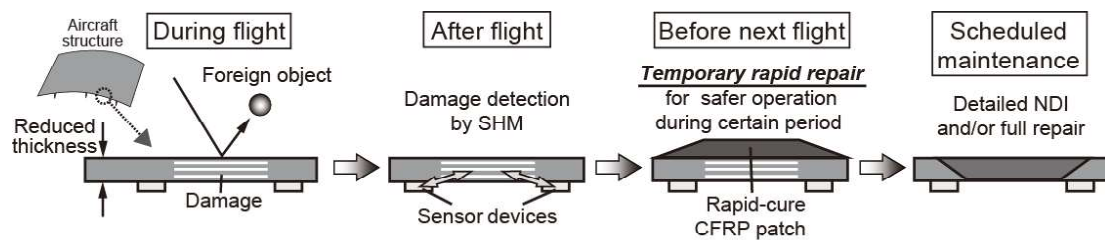


Figure 32 Ultra-lightweight structure designed based on SHM and rapid repair system [2, 3].

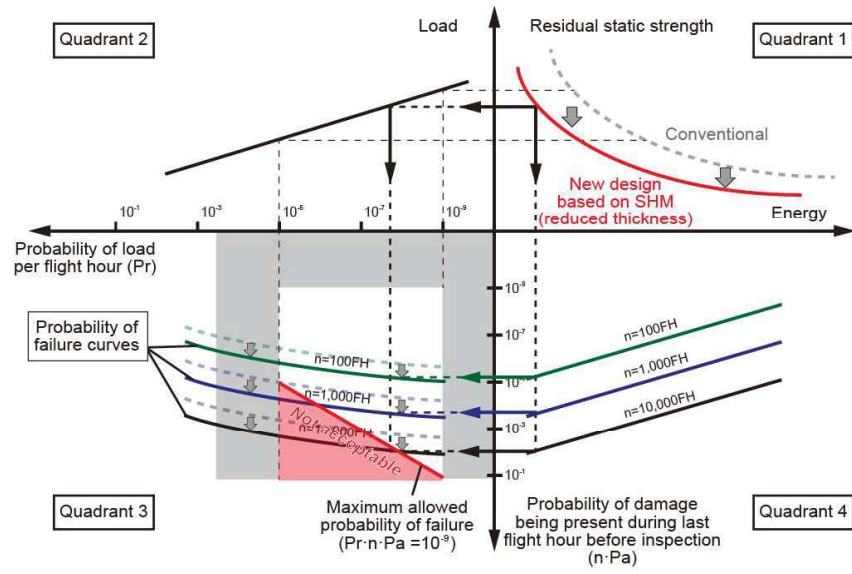


Figure 33 Failure probability of ultra-lightweight structure with reduced thickness. Probability curve (Quadrant 3) shifts downward due to decreased residual strength (Quadrant 1). However, continued safe operation is possible by using SHM and rapid repair system (Fig. 32).

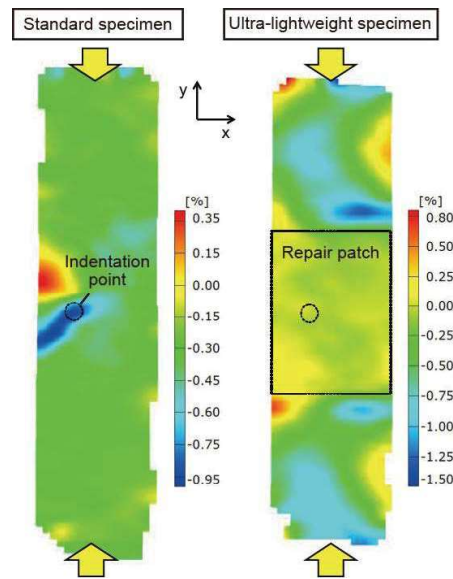


Figure 34 Strain distribution ϵ_{yy} just before failure obtained by digital image correlation. In repaired ultra-lightweight specimen, local deformation around damage was fully suppressed by repair patch, which resulted in higher strength.

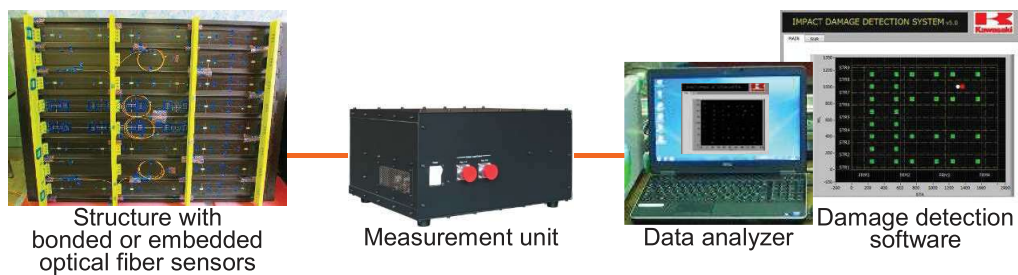


Figure 35 Impact Damage Detection system

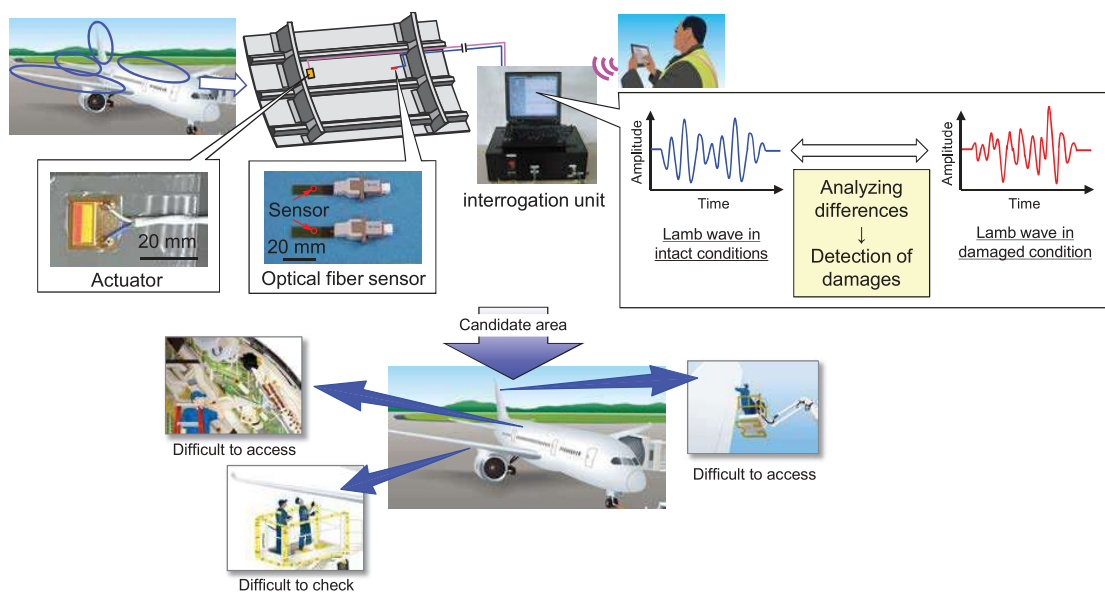


Figure 36 Overview of the SHM system.



Figure 37 The flying test bed owned by JAXA.

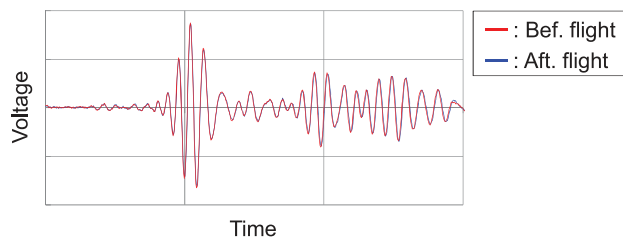


Figure 38 Result of ultrasonic Lamb wave measured in hangar.

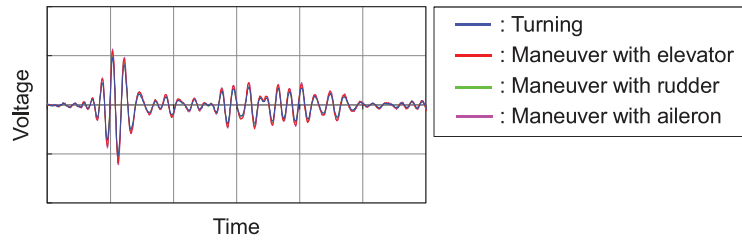


Figure 39 Result of ultrasonic Lamb waves measured during flight.

Table 4 Example data of composite material strength(Sample size n=6)

Composite material (T800H/EP:#3633)	Mechanical strength property	Sample mean (\bar{x})	Coefficient of variation (COV)	MIL-B value (x_a)	Expected reliability ($\underline{R}(x_a)$)
A: Quasi-isotropic	Open hole tension (MPa), 26°C	438	1.6%	416	0.997
B: Quasi-isotropic	Tension(MPa), 25°C	875	5.24%	737	0.996
C: Satin fabric[90] _{7s}	Interlaminar fracture toughness Mode I (KJ/m), 25°C	0.613	11.3%	0.405	0.997
D: [0] ₃₂	Interlaminar fracture toughness Mode I(KJ/m), 23°C	0.200	17%	0.0975	0.996

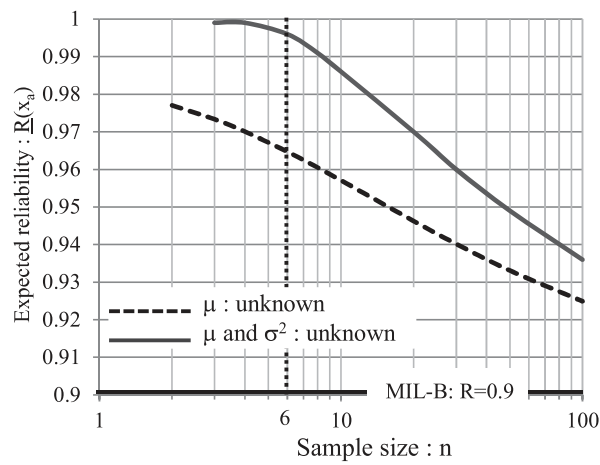


Figure 40 Bayesian expected reliability

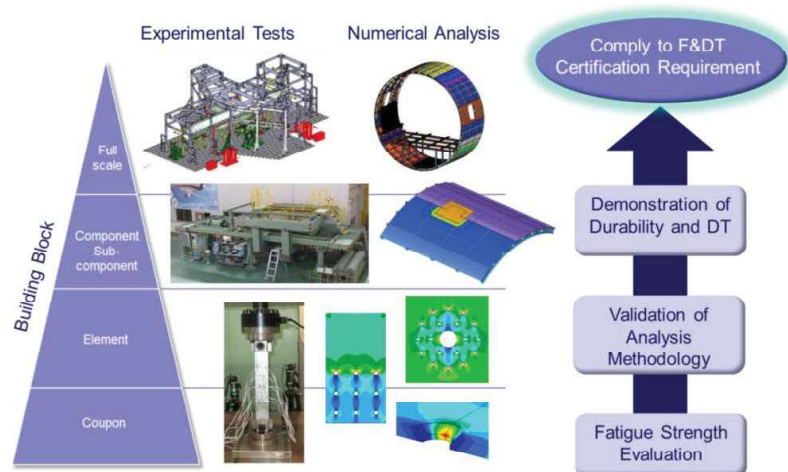


Figure 41 Building block approach for establishing SRM.

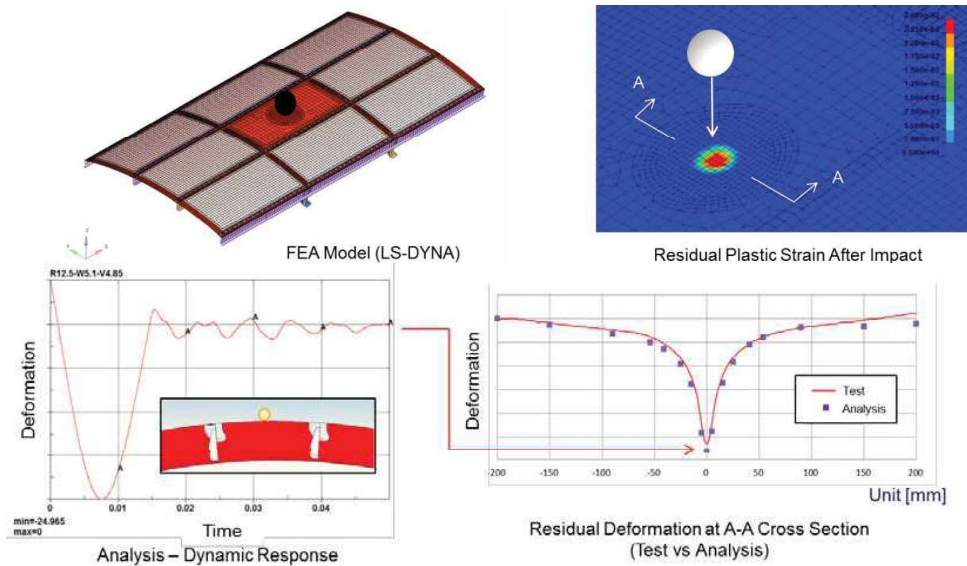


Figure 42 Simulated dynamic response and comparison of residual deformation between FEA and test.

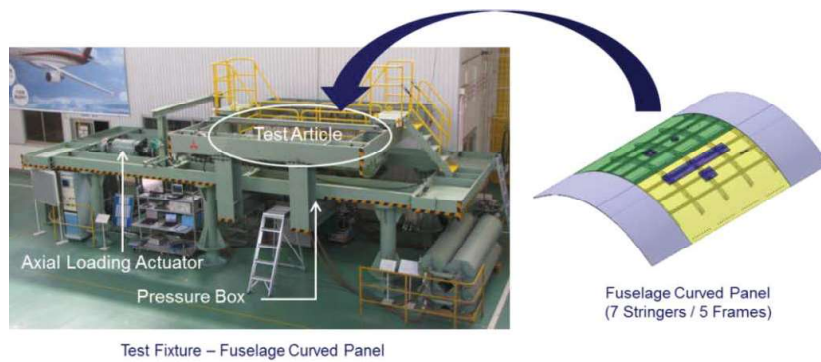


Figure 43 Combined loading fatigue test fixture for fuselage curved panel.



Figure 44 Test fixtures of XP-1 full-scale static test
(top left: XP-1 aircraft, bottom left: overview of test rig, right: test fixture of L/H wing)



Figure 45 XC-2 Aircraft

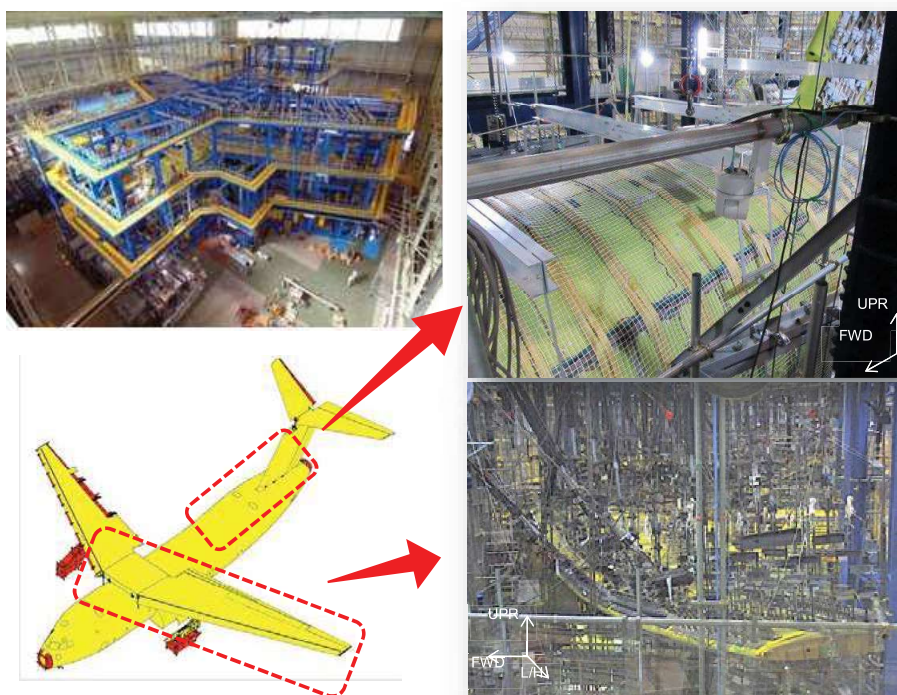


Figure 46 Test article and fixtures of XC-2 full-scale static test (top left: test rig, bottom left: FSST test article, top right: test fixtures of aft-fuselage, bottom right: test fixture of L/H wing)

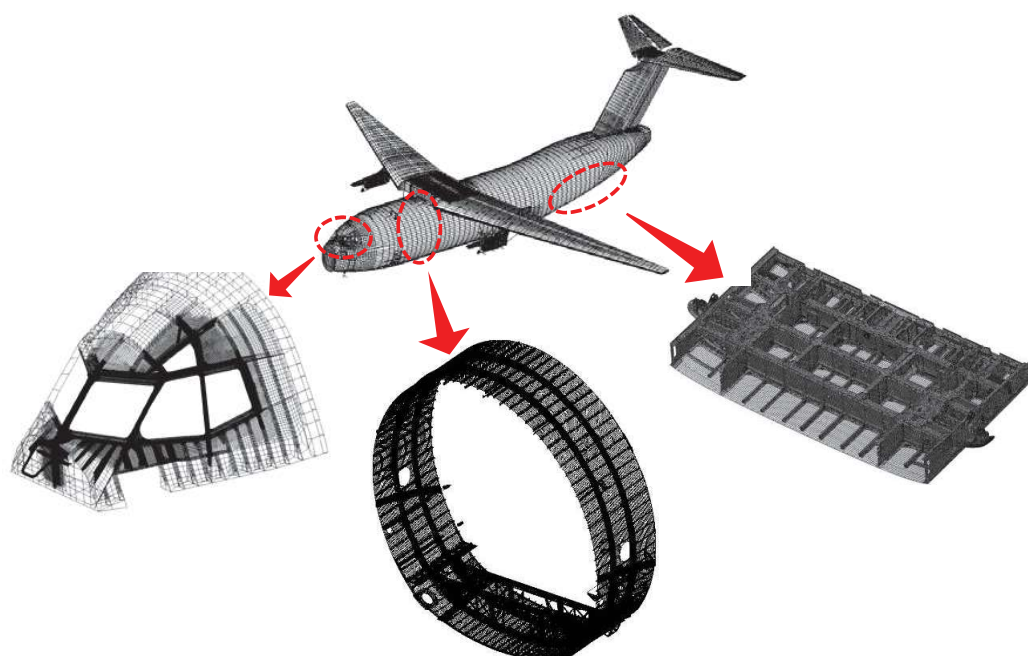


Figure 47 Finite element model of XC-2 (top: global model for aircraft-level analysis, bottom left: local model for windshield shell analysis, bottom center: local model for mid-fuselage analysis, bottom right: local model for loading ramp door analysis)



Figure 48 Advanced Technology Demonstrator (X-2)

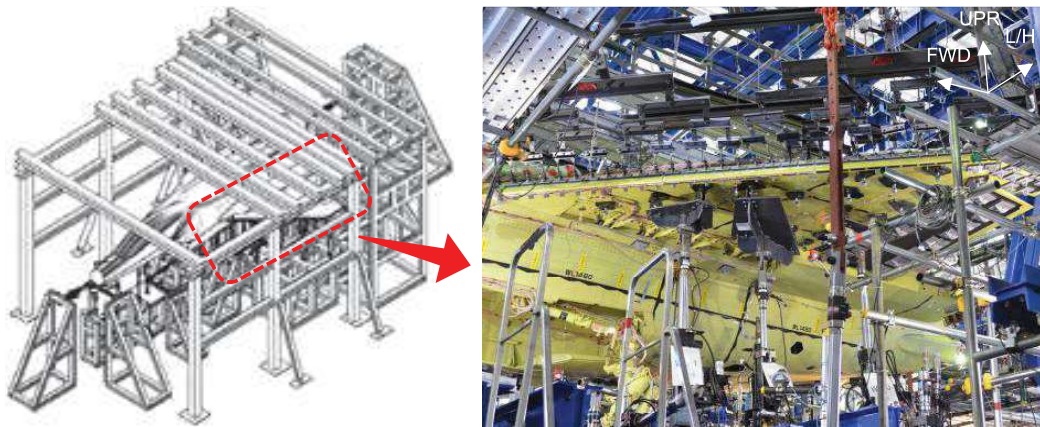


Figure 49 Full-scale static test rig configuration (left) and test setup of L/H wing for rolling pullout maneuver load condition (right)



Figure 50 Image of US-2 Firefighting Amphibian



Figure 51 Actual-size mock-up of water tank

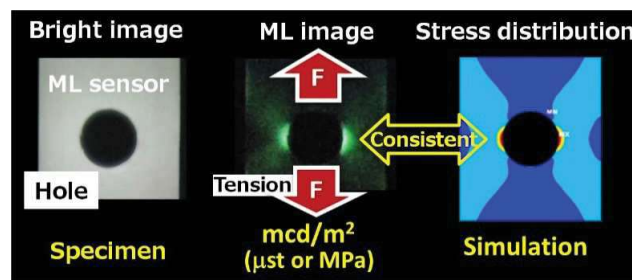


Figure 52 Feature of ML sensor

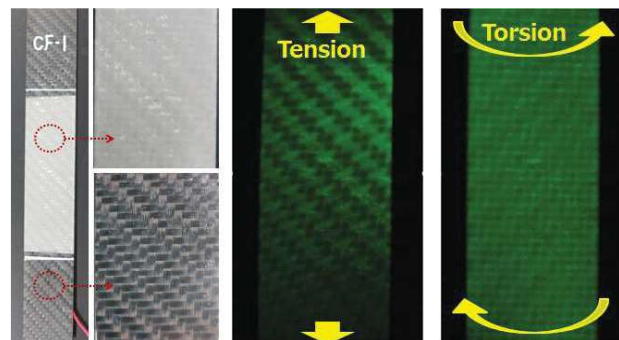


Figure 53 Visualization of strain contribution on CFRP during tensional and torsional load.

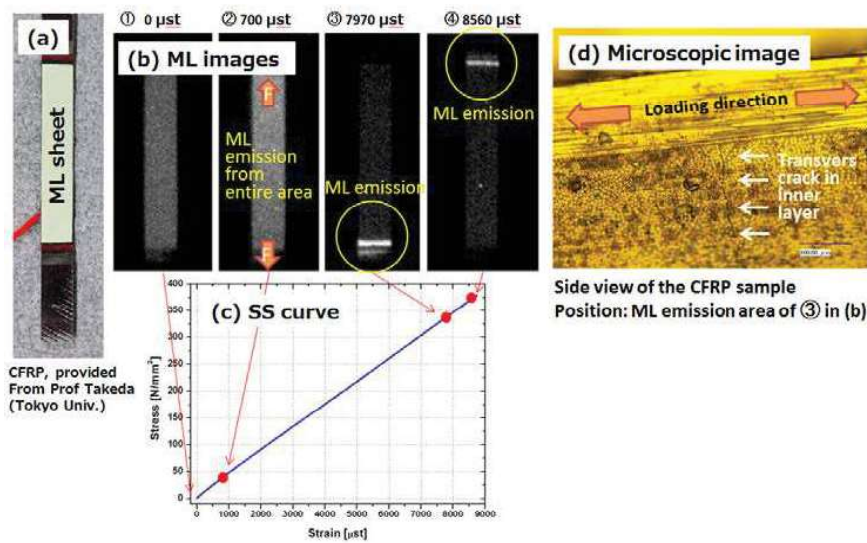


Figure 54 ML monitoring of transverse crack occurrence. (a) CFRP specimen, provided from prof. N. Takeda (Tokyo Univ.), with ML sheet. (b) ML images and (c) SS curve during tensional load application. (d) Microscopic cross sectional image at the responding area of ML emission at 7979 μs.

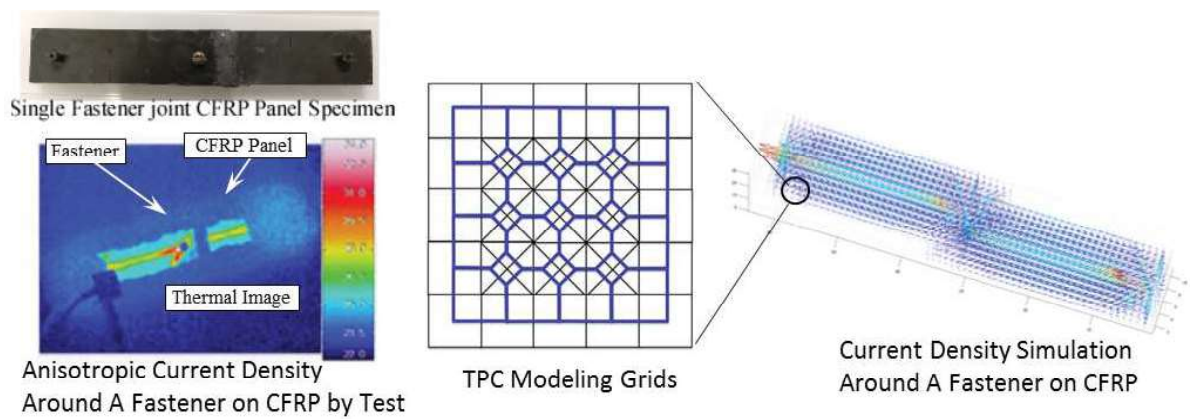


Figure 55 Tri-Prism Cell Modeling

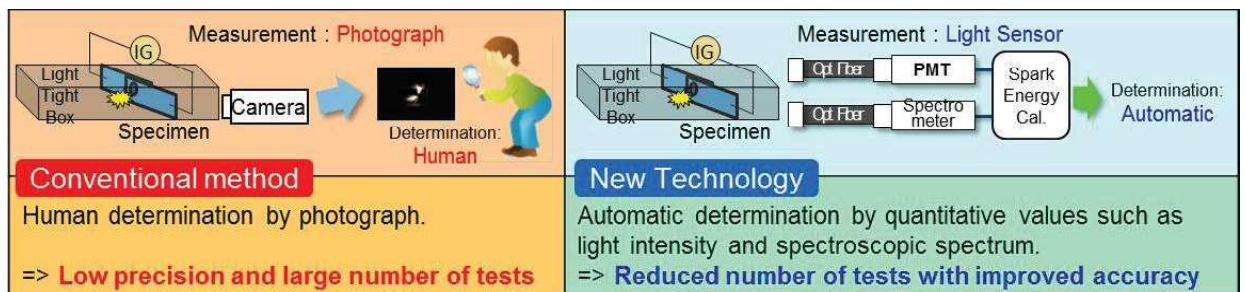


Figure 56 Ignitable Spark Detection System

Title	Fracture surface of Charpy impact test(S45C)	Material	JIS S45C MatWeb®
Experiment or Actual Equipment	Experiment	Fracture Mechanics	Brittle/Ductile
Environment	Temperature was -20-100°C in air.	How it was made.	Fracture surface was made by Charpy impact test.
Comment	These fracture surfaces were made by Charpy impact test. Material was S45C(JIS). Test temperature was, from left, -20°C, 40°C, 60°C, 80°C, 100°C. As test temperature becomes higher, an area ratio where a surface is glittering is decreasing and an area ratio where a surface is gray and shear-lip is increasing. Microscopic fracture surfaces are brittle, ductile and transition region from brittle to ductile. In the brittle picture, river pattern is observed. Strictly writing, brittle is "Quasi"-brittle. On the other hand in the ductile picture, dimples are observed.		
Remarks			

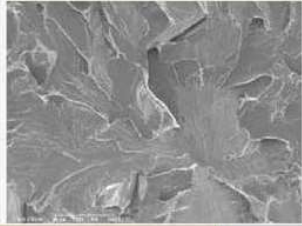
1		
		
Magnification		1200
Resolution(pixels) Image Size(μm)	Width	1200 pixels 99.96 μm
	Height	900 pixels 74.97 μm
μm/pixel		0.0833
Caption		Brittle (river pattern)

Figure 57 Example of data sheet (left): text data, (right): image data.

Table 5 Data table

Text data		Image data	
Title	Title of data sheet.	image	SEM image data.
Material	Material's name.	Magnification	Magnification observation
Experiment work or Actual Equipment	Surfaces are obtained from the experiment or equipment's failure.	Resolution and Image Size	Resolution of Image, and actual width and height of observation area.
Fracture Mechanics	Fracture mechanics detected by observer.	Interval (μm/pixel)	Actual length of a pixel.
Environment	Environment where the surface was made.	Caption	Caption for images.
How it was made.	Experimental condition or usage of actual equipment.		
Comment	Observer's comment for the surfaces.		

Table 6 Number of Accident by Type of Aircraft

Aircraft Year	Large Airplane	Small Airplane	Rotorcraft	Glider, ULP or others	Total
2015	3	9	3	12	27
2016	2	4	2	5	13

Table 7 Number of Serious Incident by Type of Aircraft

Aircraft Year	Large Airplane	Small Airplane	Rotorcraft	Glider, ULP or others	Total
2015	5	1	3	0	9
2016	5	1	4	0	10

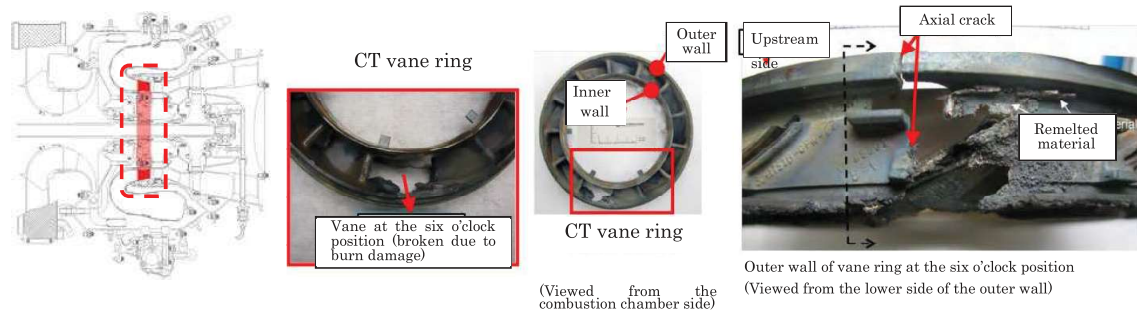


Figure 58 CT vane ring